Draft version February 5, 2008
Preprint typeset using LaTeX style emulateapj v. 11/12/01

LOCKING OF THE ROTATION OF DISK-ACCRETING MAGNETIZED STARS

M. Long, M.M. Romanova, R.V.E Lovelace
Department of Astronomy, Cornell University, Ithaca, NY 14853
Email: Long@astro.cornell.edu
Draft version February 5, 2008

ABSTRACT

We investigate the rotational equilibrium state of a disk accreting magnetized stars using axisymmetric magnetohydrodynamic (MHD) simulations. In this "locked" state, the spin-up torque balances the spin-down torque so that the net average torque on the star is zero. We investigated two types of initial conditions, one with a relatively weak stellar magnetic field and a high coronal density, and the other with a stronger stellar field and a lower coronal density. We observed that for both initial conditions the rotation of the star is locked to the rotation of the disk. In the second case, the radial field lines carry significant angular momentum out of the star. However, this did not appreciably change the condition for locking of the rotation of the star. We find that in the equilibrium state the corotation radius r_{co} is related to the magnetospheric radius r_A as $r_{co}/r_A \approx 1.2-1.3$ for case (1) and $r_{co}/r_A \approx 1.4-1.5$ for case (2). We estimated periods of rotation in the equilibrium state for classical T Tauri stars, dwarf novae and X-ray millisecond pulsars.

Subject headings: accretion, accretion disks - magnetic fields - plasma - stars: magnetic fields

1. INTRODUCTION

Disk accretion to a rotating star with a dipole magnetic field is important in a number of astrophysical objects, including T Tauri stars (Camenzind 1990; Königl 1991), X-ray pulsars (Nagase 1989; Bildsten et al. 1997), and cataclysmic variables (Warner 1995). An important property of this interaction is the disruption of the disk at the Alfvén radius, r_A, and the "locking" of the star's angular rotation at an angular velocity, Ω_{eq}, which is expected to be of the order of the disk rotation rate at the Alfvén radius, $\Omega(r_A) = (GM/r_A^3)^{1/2}$. However, the exact conditions for locking and for the value of the equilibrium rotation rate Ω_{eq} (when the star does not spin up or spin down) were not been established.

One of the complicated aspects of the disk-magnetosphere interaction is the process of angular momentum transport between the disk and the magnetized star. In the first models of the disk-magnetosphere interaction it was proposed that the magnetic field has a dipole configuration everywhere and that the net change between spin-up torque which arises from the magnetic connection of the star to the disk within the corotation radius r_{co} and the spin-down torque which arises from the connection beyond the corotation radius determines the spin evolution of the star (Ghosh, Lamb & Pethick 1977; Ghosh & Lamb 1978, 1979 - hereafter GL79). The corotation radius is the radius where the disk rotates at the same speed as a star, $r_{co} = (GM/\Omega_*^2)^{1/3}$. It was suggested that for a particular value of the star's rotation rate, Ω_{eq}, the positive spin-up torque balances the negative spin-down torque and the star is in the rotational equilibrium state (Ghosh & Lamb 1978, 1979; Wang 1995).

Recent studies of the evolution of the magnetic field threading the disk and the star led to understanding that the field tends to be inflated and possibly opened due to the difference in the angular velocities of the foot-points (Lovelace, Romanova & Bisnovatyi-Kogan 1995 - hereafter LRBK; Shu et al. 1994; Bardou 1999, Uzdensky, Königl & Litwin 2002). In this case a star may lose some angular momentum through the open field lines and the equilibrium state will be determined by the balance between processes of spin-up/spin-down associated with the disk-magnetosphere interaction, and spin-down associated with the open field lines.

In some models it was suggested that the angular momentum transport between the star and the disk may be much less efficient (Agapitou & Papaloizou 2000) if the field lines are opened as proposed by LRBK. Under such conditions the rotational equilibrium state will be quite different (e.g., Matt & Pudritz 2004, 2005). The goal of this paper is to derive the conditions for the rotational equilibrium state using axisymmetric MHD simulations of the disk-magnetosphere interaction.

The properties of the rotational equilibrium state depend on the configuration of the magnetic field threading the star and the disk. Consequently, analysis of this problem requires two or three dimensional simulations. Axisymmetric simulations have shown that the field lines do open (Hayashi et al. 1996; Miller & Stone 1997; Hirose et al. 1997; Romanova et al. 1998; Fendt & Elstner 1999). However, longer runs have shown that the innermost field lines reconnect to form a closed magnetosphere, and some of them open and close again in a recurrent manner (Goodson & Winglee 1997; Goodson, Winglee & Böhm 1999; Romanova et al. 2002, hereafter RUKL; Romanova et al. 2004; Kato et al. 2004, Von Rekowski & Brandenburg 2004). Detailed simulations of the slow, viscous disk accretion to a rotating star with an aligned dipole field (RUKL) have shown that on long time-scales, the magnetic field lines in the vicinity of the Alfvén radius r_A are closed or only partially open, and these lines are important for the angular momentum transport between the star and the disk. The balance between the magnetic flux in closed and open field lines is clearly important for determining the rotational equilibrium state.

In RUKL, a preliminary search for the conditions of

torqueless accretion was performed and the torqueless accretion was shown to exist. In this paper, we give a detailed study of the conditions for torqueless accretion using an improved axisymmetric MHD code which makes possible longer simulation runs compared to RUKL. The main question is: What is the angular rotation rate of a star Ω_{eq} for the torqueless accretion given the star's mass M, magnetic moment μ, and accretion rate $\dot{M}$. Equivalently, if we know the Alfvén radius r_A, then what is the corotation radius r_{co} in the rotational equilibrium state? In earlier theoretical models, it was estimated that the critical fastness parameter $\omega_s = \Omega_*/\Omega_K(r_A) = (r_A/r_{co})^{3/2}$ of the equilibrium state is in the range of $0.47 - 0.95$ (Li & Wickramasinghe 1997). This corresponds to the ratio $r_{co}/r_A \sim 1.1 - 1.7$.

In this paper we determine the value of r_{co}/r_A for torqueless accretion numerically by performing a large set of numerical simulations for different values of Ω_*, μ, $\dot{M}$, and disk/corona parameters. We also investigated the matter flow and the angular momentum transport in the equilibrium state. In §2, the numerical model is described. We focus on conditions where the torqueless accretion occurs and study its dependence on different physical parameters for different cases in §3 and 4. In §5, we apply our results to relevant objects, such as CTTSs, cataclysmic variables, and X-ray millisecond pulsars. We discuss results in Section 6.

2. THEORETICAL IDEAS AND NUMERICAL SIMULATIONS

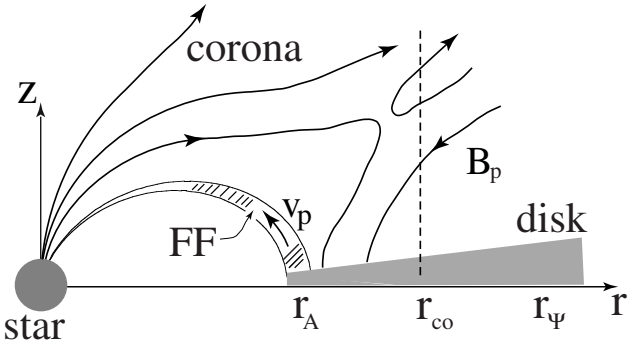

FIG. 1.— Sketch of disk accretion to a star with an aligned dipole magnetic field, where r_A is the Alfvén radius, r_{co} is corotation radius, r_Ψ is the deviation radius where a significant deviation from Keplerian rotation occurs for $r < r_\Psi$ due to the magnetic force on the disk. The dashed line divides the rapidly rotating region and the slowly rotating region. FF denotes the funnel flow.

Theoretical aspects of the disk-magnetoshpere interaction were developed in the 1970s (e.g. Pringle & Rees, 1972; Ghosh, Lamb & Pethick 1977; GL79). As sketched in Figure 1, the initial Keplerian accretion disk is threaded by the star's magnetic field. The inner radius of the disk, referred to as the Alfvén radius r_A, occurs at the radial distance where the energy-density of matter in the disk equals to magnetic energy-density, or where the paramter $\beta = \rho v^2/(B^2/8\pi) = 1$. (e.g., Lamb, Pethick & Pines 1973; Davidson & Ostriker 1973). We observed from many simulations that the inner radius of the disk coincides with this radius. The Alfvén radius is usually derived analytically using a number of approximations. For a dipole magnetic field of the star, $\mu \equiv B_* R_*^3 = B r^3$,

$$r_A = k_A r_A^{(0)} = k_A \frac{\mu^{4/7}}{(2GM)^{1/7}\dot{M}^{2/7}} \ . \quad (1)$$

Here, G is the gravitational constant, $\dot{M}$ is the mass accretion rate, M is the mass of the star, $r_A^{(0)}$ is the Alfvén radius for the spherical accretion (Elsner & Lamb 1977). The coefficient k_A accounts for the fact that the disk accretion is different from spherical accretion. Using values of the different parameters obtained from our simulations we obtained $r_A^{(0)}$ and then compared it with r_A. From this we obtained $k_A \approx 0.5$.

In a somewhat different approach, Wang (1995) suggested that the disk stops or disrupts at the radius r_0 where the magnetic and matter stresses are equal, $(-r^2 B_\phi B_z)_0 = \dot{M}[\mathrm{d}(r^2\Omega)/\mathrm{d}r]_0$, where the 0−subscripts indicate evaluation at $r = r_0$, B_ϕ and B_z are the components of the magnetic field, Ω is the angular velocity of the disk. We took values of parameters from our simulations and derived the radius the radius r_0. We observed that this radius approximately coincides with r_A.

Whether a star spins up or spins down is due to angular momentum flow to or out of the star transported by the matter flow and the magnetic field. Some field lines of the star thread the disk and transport angular momentum between the disk and the star (e.g., GL79). Other field lines are inflated and become open, that is, not connected to the disk. These open field lines may transport angular momentum away from the star to the corona without direct interaction with the disk (Agapitou & Papaloizou 2000; Matt & Pudritz 2004). We observed that both closed and open field lines contribute to the angular momentum transport to the star.

For the case where the poloidal field lines connect the star and the disk, the field lines passing through the disk within the corotation radius r_{co} spin up the star, while the field lines passing through the disk at large distances spin it down (GL79). The dashed vertical line in Figure 1 at r_{co} divides the regions which provide positive and negative torques. There is also a region $r \lesssim r_\Psi$ where the magnetic interaction modifies the Keplerian rotation of the disk, and where the angular momentum transport between the star and the disk is important (GL79, RUKL). If some of the magnetic field lines are open, then angular momentum may be also transported outward from the disk and from the star through twisting of open magnetic field lines. Thus part of the angular momentum flux may be transported by the matter flow, part by the open field lines, and part by closed field lines connecting the star and the disk.

2.1. *Main Equations*

The disk-magnetoshpere interaction is considered to be described by the MHD equations,

$$\frac{\partial \rho}{\partial t} + \nabla \cdot (\rho \mathbf{v}) = 0 \ , \quad (2)$$

$$\rho \frac{\mathrm{d}\mathbf{v}}{\mathrm{d}t} = -\nabla p + \rho\, \mathbf{g} + \frac{1}{4\pi}(\nabla \times \mathbf{B}) \times \mathbf{B} + \mathbf{F}^{vis} \ , \quad (3)$$

$$\frac{\partial \mathbf{B}}{\partial t} = \nabla \times (\mathbf{v} \times \mathbf{B}) \ , \quad (4)$$

$$\frac{\partial (\rho S)}{\partial t} + \nabla \cdot (\rho \mathbf{v} S) = 0 \ , \quad (5)$$

$$\nabla \cdot \mathbf{B} = 0 \ . \tag{6}$$

Here, $S = p/\rho^\gamma$ is the entropy per gram, $\mathbf{g}$ is the gravitational acceleration, $\mathbf{F}^{vis}$ is the viscous force. The viscosity model of Shakura and Sunyaev (1973) is used with viscosity coefficient $\nu = \alpha c_s^2/\Omega_K$, where $c_s = (\gamma p/\rho)^{1/2}$ is the sound speed, and parameter α is dimensionless with values $\alpha \sim 0.01 - 0.03$ considered here.

Equations 2-6 were solved with a Godunov-type numerical code developed by Koldoba, Kuznetzov & Ustyugova (1992) (see also Koldoba & Ustyugova 1994; Ustyugova et al. 1995). We used an axisymmetric spherical coordinates with a grid $N_r \times N_\theta = 131 \times 51$. Test simulations with larger or smaller grids were also performed.

2.2. *Reference Units*

We let R_0 denote a reference distance scale, which is equal to $R_*/0.35$ where R_* is the radius of the star. The subscript "0" denotes reference values for units. We take the reference value for the velocity, $v_0 = (GM/R_0)^{1/2}$, the angular speed $\Omega_0 = v_0/R_0$, the timescale $P_0 = 2\pi R_0/v_0$, the magnetic field $B_0 = B_*(R_*/R_0)^3$, the magnetic moment $\mu_0 = B_0 R_0^3$, the density $\rho_0 = B_0^2/v_0^2$, the pressure $p_0 = \rho_0 v_0^2$, the mass accretion rate $\dot{M}_0 = \rho_0 v_0 R_0^2$, and the angular momentum flux $\dot{L}_0 = \rho_0 v_0^2 R_0^3$. The dimensionless variables are $\widetilde{R} = R/R_0$, $\widetilde{v} = v/v_0$, $\widetilde{T} = T/P_0$ etc. In the following we use these dimensionless units but the tildes are implicit.

2.3. *Boundary and Initial Conditions*

Boundary conditions: At the inner boundary $R = R_*$, "free" boundary conditions are applied for the density, pressure, entropy, velocity, and $\phi-$component of the magnetic field, $\partial\rho/\partial R = 0$, $\partial p/\partial R = 0$, $\partial S/\partial R = 0$, $\partial(\mathbf{v} - \mathbf{\Omega} \times \mathbf{R})_R/\partial R = 0$, $\partial(RB_\phi)/\partial R = 0$. The poloidal components B_R and B_θ are derived from the magnetic flux function $\Psi(R, \theta)$, where Ψ at the boundary is derived from the frozen-in condition $\partial\Psi/\partial t + \mathbf{v}_p \cdot \nabla\Psi = 0$. At the outer boundary, free boundary conditions are taken for all variables. The outer boundary was placed far away from the star in order to diminish the possible influence of this boundary (Ustyugova et al. 1999).

Initial conditions: The star has a fixed aligned dipole magnetic field with magnetic moment μ. The initial accretion disk extends inward to an inner radius r_d, and it has a temperature T_d which is much less than the temperature of the corona T_c. The initial disk and corona are in pressure balance. The corona above the disk rotates with the angular velocity of the disk in order to avoid a rapid initial shearing of the magnetic field. The initial density distributions in the disk and corona are constrained by the condition that there is a balance of pressure gradient, gravitational and centrifuge forces. This balance is necessary in order to have smooth accretion flow which evolves on the viscous time scale of the disk (see details in RUKL). To avoid a very strong initial interaction of the disk with the magnetic field, we take the initial inner radius of the disk at $r_d = 6$ or $r_d = 5$, far away from the star.

In order to investigate the rotational equilibrium states, we performed simulations with two types of initial conditions, type I and type II. For type I initial conditions we have a magnetic field which is relatively weak, $\mu = 2$, the disk is relatively thick with fiducial density $\rho_d = 1$, and relatively high coronal density, $\rho_{cor} = 0.005$. The initial inner disk radius is $r_d = 6$. The outer radius of simulation domain corresponds to $18R_0$, that is, about $54R_*$. Results for this case are described in §3. For type II initial conditions the star's magnetic field is much stronger, $\mu = 10$, the coronal density is much lower $\rho_{cor} = 0.001$, the disk is thinner, and the initial inner disk radius is $r_d = 5$. The outer radius of simulation domain corresponds to $68R_0$, that is, about $136R_*$.These initial conditions, which are more favorable for inflation and opening of the coronal field lines, are described in §4.

3. THE EQUILIBRIUM STATE OF DISK ACCRETION FOR INITIAL CONDITIONS OF TYPE I

3.1. *Search for Rotational Equilibrium State*

Whether the star spins up or spins down is determined by the net flux of angular momentum to the surface of the star, $\dot{L}$. This flux is composed of two parts, the flux carried by the matter $\dot{L}_m$, and that carried by the magnetic field, $\dot{L}_f$:

$$\dot{L} = \dot{L}_m + \dot{L}_f \ , \tag{7}$$

$$\dot{L}_m = -\int \mathrm{d}\mathbf{S} \cdot \rho r v_\phi \mathbf{v}_p \ , \tag{8}$$

$$\dot{L}_f = \frac{1}{4\pi} \int \mathrm{d}\mathbf{S} \cdot r B_\phi \mathbf{B}_p \ , \tag{9}$$

where the $p-$subscript denotes the poloidal component, and $\mathrm{d}\mathbf{S}$ is the outward pointing surface area element of the star. We performed a set of simulations for different angular velocities of the star, Ω_*, to find the critical value of Ω_*, corresponding to the rotational equilibrium state, that is, the state when $\dot{L} \approx 0$. Other parameters $(\dot{M}, \mu)$ were fixed.

We observed that $\dot{L}_f$ is always dominant over $\dot{L}_m$ for all cases (as in RUKL) and thus we compared $\dot{L}_f$ for these cases. This was predicted in earlier theoretical research (e.g., GL79). We narrowed the set of Ω_* values so that $\dot{L}_B$ was very small on average (see Figure 2a). Among these we picked the one for which $\dot{L}_f \approx 0$ that corresponds to the rotational equilibrium state, $\Omega_* = \Omega_{eq}$. For this case, the corotation radius $(r_{co})_{eq} \approx 1.7$.

In addition, we calculated matter flux to the star,

$$\dot{M} = -\int \mathrm{d}\mathbf{S} \cdot \rho \mathbf{v}_p. \tag{10}$$

Figure 2b shows the mentioned fluxes in the rotational equilibrium state. Note that this state is typically reached at $T > 50$ because initially the disk is far from the magnetosphere and it takes time for the disk to move inward. One can see that the angular momentum flux carried by the field $\dot{L}_f$ fluctuates around zero.

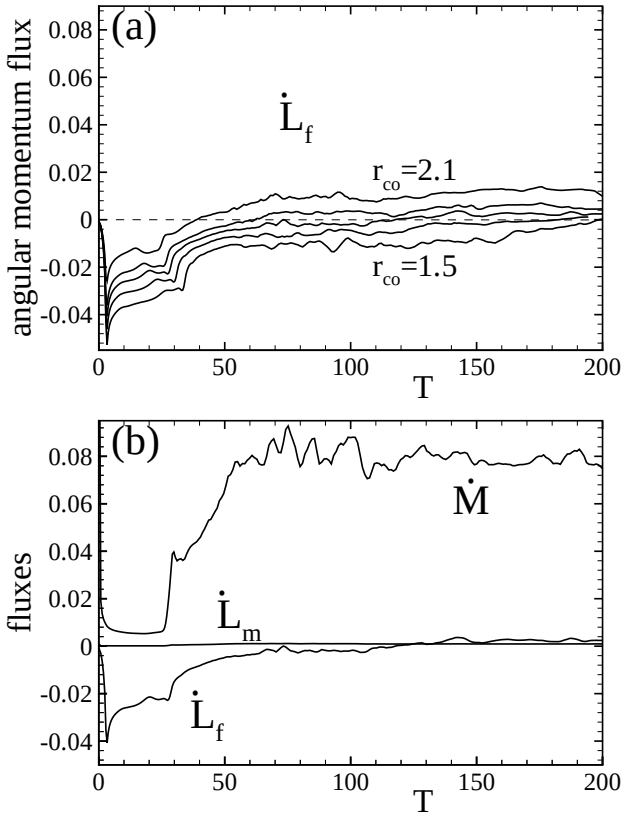

FIG. 2.— (a) The evolution of $\dot{L}_f$ for different corotation radii from $r_{co} = 1.5$ (bottom line) to $r_{co} = 2.1$ (top line); (b) The evolution of $\dot{M}$ and the angular momentum fluxes carried by matter $\dot{L}_m$ and the magnetic field $\dot{L}_f$ in rotational equilibrium state, $r_{co} \approx 1.7$. Time scale is P_0 (see §2.2).

3.2. *Disk-Magnetosphere Interaction in Equilibrium State*

We now discuss in more detail the rotational equilibrium state where $r_{co} = 1.7$. Figure 3a shows the evolution of matter and the magnetic flux with time. One can see that initially the disk matter moves inward, then it stops near magnetosphere and goes to the star through a funnel flow which is driven up by pressure gradient force (RUKL;Koldoba et al. 2002). The funnel flow is quasi-stationary after a time $T \sim 50$. The bold red line divides the regions where magnetic and matter energy densities dominate, that is, the line where $\beta = 1$ (see §2). The corresponding Alfvén radius is $r_A \approx 1.2 - 1.3$. We also estimated the radius r_0 derived from the equality of magnetic and matter stresses. We observed that this radius is close to r_A, $r_0 \approx 1.3 - 1.4$.

Figure 3a shows that the magnetic field for $r > r_A$ is strongly non-dipolar, and the structure of the field is complicated. The magnetic field lines initially inflate for $T < 30$; however, later some of them reconnect forming closed field lines and thus enhancing the dipole component in the closed magnetosphere. Other field lines, which are near the axis stay open and represent the lines of "magnetic tower", which is often observed in different simulations of the disk-magnetosphere interaction (e.g., Kato et al. 2004; Romanova et al. 2004). Many field lines are radially stretched by the accreting matter. These field lines are located in the disk and above the disk. Most of these field lines are connected to the star. The field lines above the closed magnetosphere continue to open and reconnect in quasi-periodic manner. In case of the lower density corona (see §4), inflation is more efficient, and this leads to larger quasi-periodic oscillations of the magnetic flux and associated fluxes.

We analyzed the angular momentum transport between the star and the disk and corona. Figure 3b shows the distribution of the angular momentum fluxes carried by the field $\mathbf{f}_B = rB_\phi \mathbf{B}_p/4\pi$ (left panel) and carried by the matter $\mathbf{f}_m = -\rho r v_\phi \mathbf{v}_p$ (right panel). One can see that for $r > r_A$, most of the angular momentum flux is carried by the matter (see the region with the high positive angular momentum at the right panel). However, for $r \lesssim r_A$ it is mainly transported by the magnetic field (see left panel of Figure 3b). The streamlines in the Figure 3b show direction of the flow of angular momentum. One can see that matter always carries positive angular momentum towards the star, which tends to spin up the star. Magnetic field lines carry angular momentum out of the star through the field lines threading the area of the funnel flow and corona. The situation with the angular momentum transport seems to be more complicated compared to one described by GL79.

The angular momentum fluxes change with distance and with angle. We calculated the angular distribution of fluxes $F_B(r,\theta) = 2\pi r^2 \sin\theta \mathbf{f}_B \cdot \hat{r}$ and $F_m(r,\theta) = 2\pi r^2 \sin\theta \mathbf{f}_m \cdot \hat{r}$ through the spheres of different radii r. Figure 4 shows that at a large radius, $r = 1.8$, matter carries most of the angular momentum, while the magnetic field also contributes but with the opposite sign. At smaller radii, the fluxes become smaller and the largest flux is in the region of the funnel flow. At the surface of the star, the flux associated with matter is very small. The flux associated with the field has two components of the opposite sign which cancel each other approximately.

The distribution of angular momentum flux is more complicated compared to that of theoretical models. However, the equilibrium state does exist and the ratio r_{co}/r_A is not very much larger than unity. This means that the rotation of the star is efficiently locked to the rotation of the inner regions of the disk.

One can see from Figure 3a, that a significant part of the disk is disturbed by the disk-magnetosphere interaction. Figure 5 shows the distribution of the angular velocity of the disk in the equatorial plane. We observed that the angular velocity varies around the Keplerian value and is usually slightly smaller then Keplerian. The magnetic field is strongly wound up in the disk so that the azimuthal field dominates. The inner regions of the disk $r \lesssim r_\Psi \sim 4$ are appreciably influenced by the magnetic field.

3.3. *Dependence on μ and α*

Next, we took a star in the rotational equilibrium state ($r_{co} = 1.7$) and varied the magnetic moment of the star μ. Figure 6a shows that when μ increases, the rate of change of angular momentum of the star becomes more negative, that is a star spins-down. This is connected with the fact that for larger μ, the magnetosphere is larger and the flux of the positive angular momentum to the star is smaller than in the equilibrium state. For example, for $\mu = 4$, the inner disk radius is at $r_A \approx 1.6$. At this in-

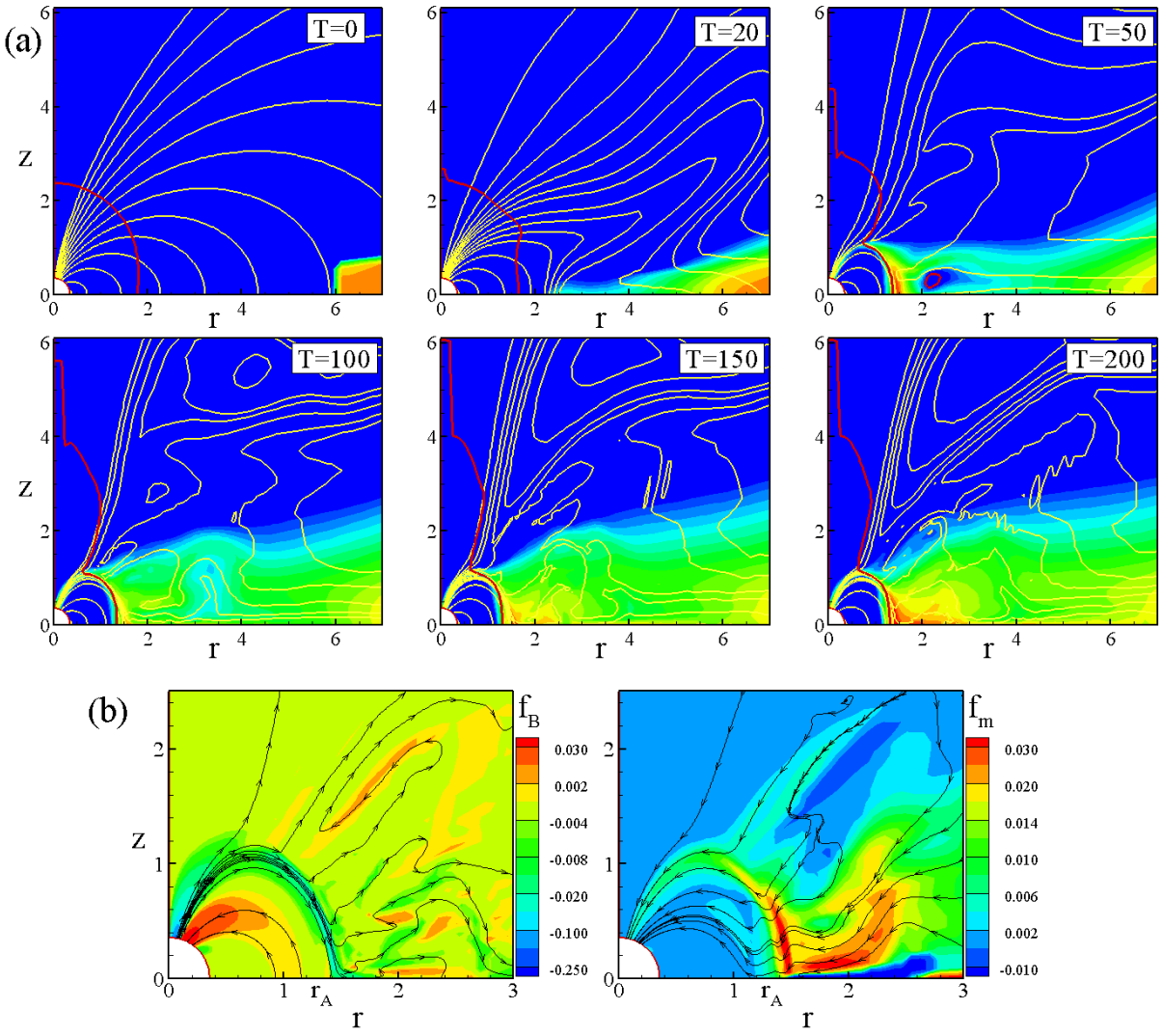

FIG. 3.— (a). Evolution of the density (color background), and the magnetic field (yellow lines) in rotational equilibrium state for type I initial conditions for $T = 0 - 200$ rotations. The density changes from $\rho = 2$ in the disk to $\rho = 0.005$ in the corona. The bold red line corresponds to $\beta = 1$ (see §2). (b). Fluxes of angular momentum carried by magnetic field $\mathbf{f}_B$ (left panel) and by matter $\mathbf{f}_m$ (right panel) at $T = 200$. Color background shows value of the fluxes, the streamlines with arrows - the direction of the angular momentum flow.

ner radius, the disk rotates much slower than the star and a star strongly spins down. Roughly, the dependence is

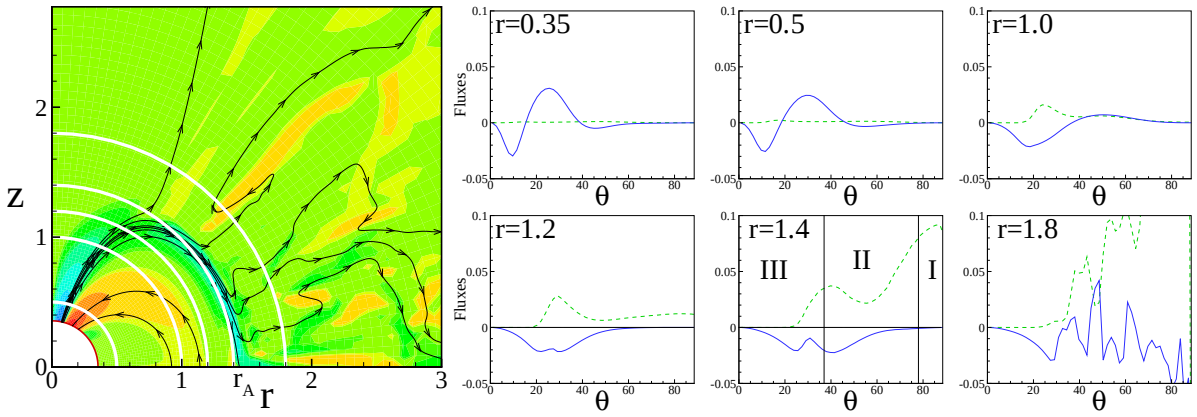

FIG. 4.— Angular distribution of fluxes $F_m(r,\theta)$ and $F_B(r,\theta)$ for type I initial conditions. The left-hand panel shows radii along which the angular momentum fluxes are calculated. The right-hand panel shows the angular momentum fluxes carried by the magnetic field (solid lines) and the matter (dashed lines) at different radii r. The numbers show the regions where the angular momentum flux carried by the field is carried mostly by the closed (I), radial (II), or open (III) field lines.

$\dot{L}_f \sim -0.02\mu + 0.04$. The balance between spin-up and spin-down torques is similar to that suggest by the GL79 model, where positive and negative torques are associated with regions within and beyond the corotation radius. We also observed different regions contributing positive and negative angular momentum fluxes. However now the distribution of the external to the Alfvén surface field lines is more complicated.

We calculated the average value of r_A for each μ and obtained the dependence $r_A \sim \mu^{\kappa}$, with $\kappa = 0.36$. This coefficient κ is somewhat different from that of equation (1) where $k = 4/7 \approx 0.57$. The difference may be connected with the fact that in the theoretical analysis the magnetic field is assumed to be a pure dipole field everywhere, whereas the simulations show that the actual field is different from a dipole for $r \gtrsim r_A$. In this and all above simulations, the viscosity coefficient was fixed at the value $\alpha = 0.02$.

We also performed simulation runs for different values of the disk viscosity, $\alpha = 0,\ 0.01,\ 0.02$, and 0.03, with other parameters fixed. We observed that for larger α the accretion rate is larger, and the Alfvén radius r_A is smaller. Thus, the region of positive torque becomes larger than the region of negative torque, and $\dot{L}_f$ is larger. In other words, at a higher accretion rate $\dot{M}$, incoming matter brings more of positive angular momentum, which is transferred to larger angular momentum flux carried by the field $\dot{L}_f$. The angular momentum flux increases with α (see Figure 6b) as about $\dot{L}_f \sim \alpha^{1.9}$ for $\alpha \geq 0.01$.

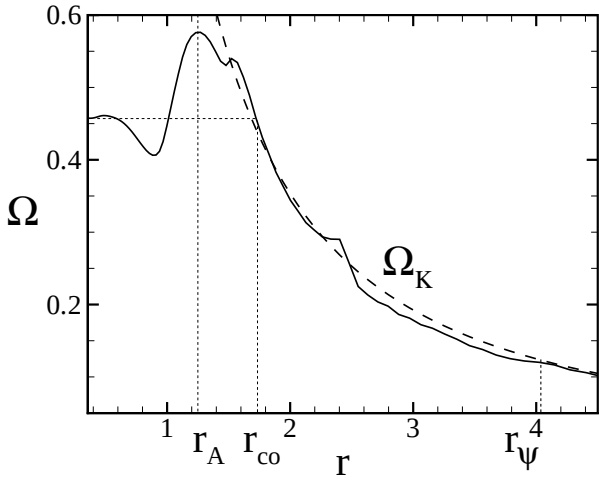

FIG. 5.— Radial distribution of angular velocity of the disk along in the equatorial plane at $T = 180$. The dash line shows Keplerian angular velocity.

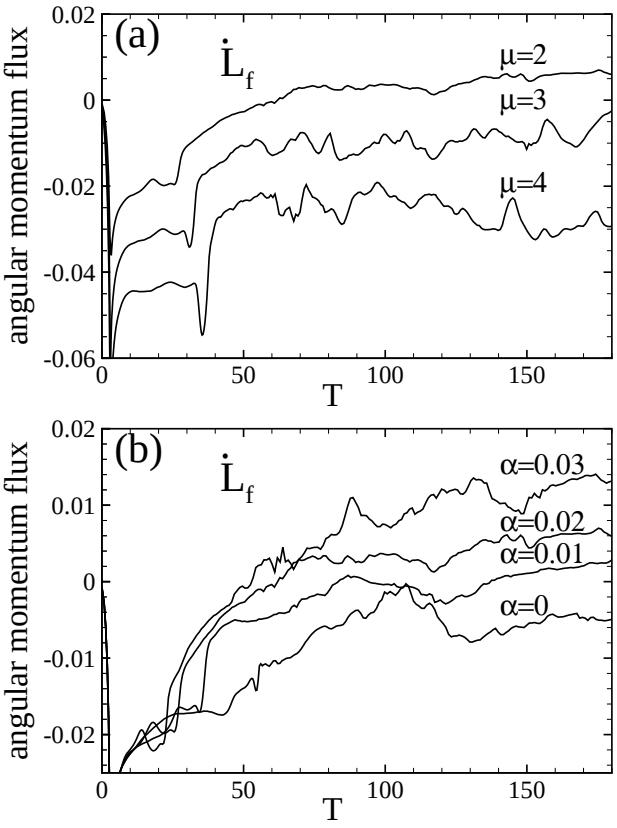

FIG. 6.— (a) The evolution of the angular momentum flux to the star carried by the magnetic field $\dot{L}_f$ for different magnetic moments of the star μ with other parameters fixed. (b) The evolution of the angular momentum flux carried by magnetic field $\dot{L}_f$ for different values of of the disk viscosity α with other parameters fixed.

4. EQUILIBRIUM STATE OF DISK ACCRETION FOR INITIAL CONDITIONS OF TYPE II

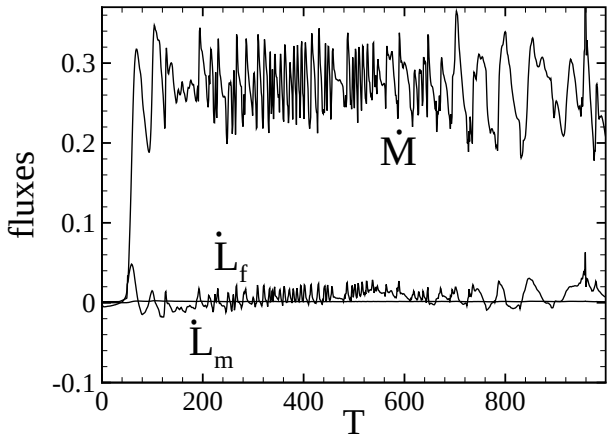

FIG. 7.— The evolution of the matter flux $\dot{M}$ and the angular momentum fluxes carried by matter $\dot{L}_m$ and magnetic field $\dot{L}_f$ in the rotational equilibrium state for the type II initial conditions.

Here we consider another case corresponding to quite different initial conditions referred to as type II. This case has a stronger magnetic field, $\mu = 10$, and a much lower coronal density, $\rho_{cor} = 0.001$. The density in the corona influences the evolution of the magnetic field in the corona, namely, the inflation and opening of the magnetic field

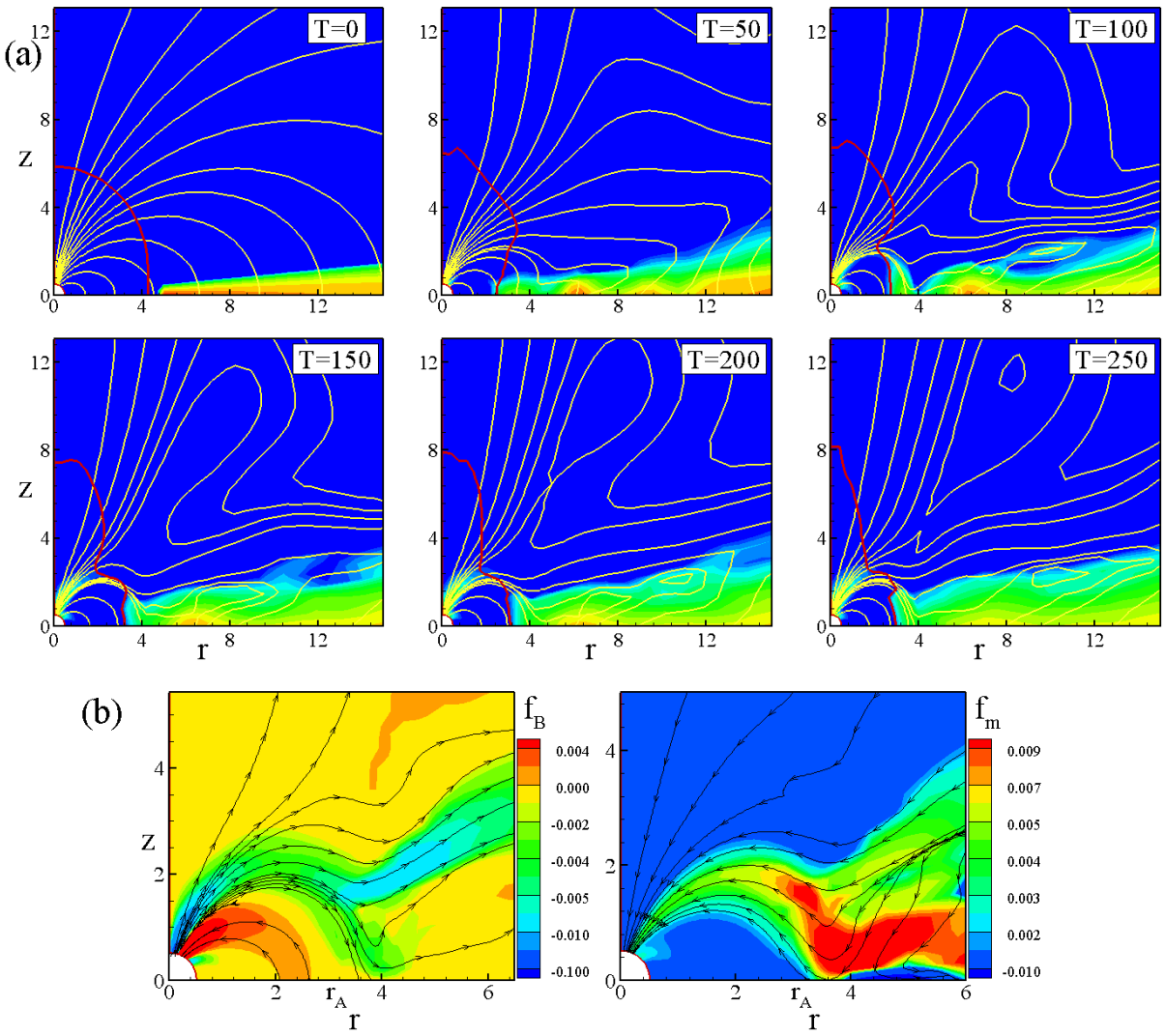

FIG. 8.— (a). Evolution of the density (color background), and the magnetic field lines (yellow lines) in rotational equilibrium state of type II initial conditions for $T = 0 - 250$ rotations. The density changes from $\rho = 2$ in the disk to $\rho = 0.001$ in the corona. The bold red line corresponds to $\beta = 1$ (see §2). (b). Fluxes of angular momentum carried by magnetic field $\mathbf{f}_B$ (left panel) and by matter $\mathbf{f}_m$ (right panel) at $T = 250$. Color background shows value of the fluxes, the streamlines with arrows - the direction of the angular momentum flow.

lines is favored. As discussed earlier, the angular momentum transport between the disk and star occurs in part

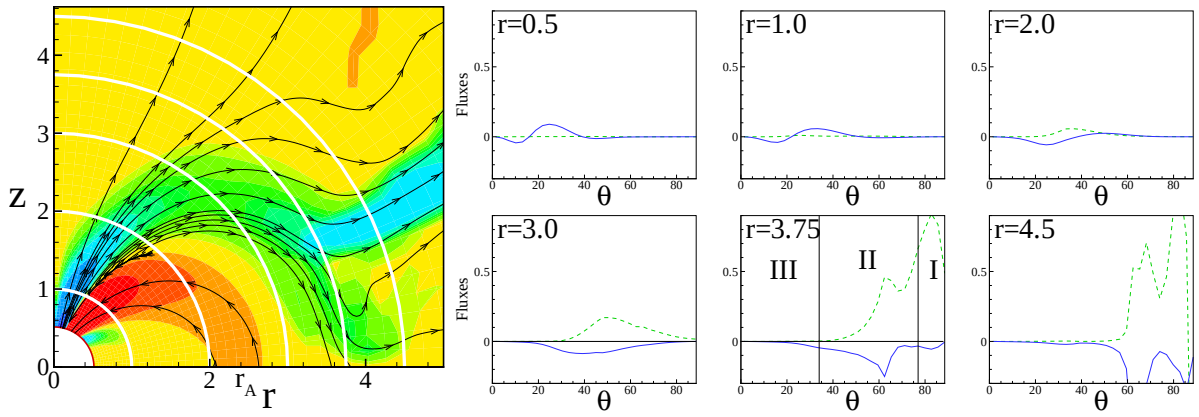

FIG. 9.— Angular distribution of fluxes $F_m(r,\theta)$ and $F_B(r,\theta)$ for initial conditions of type II. The left-hand panel shows radii along which the angular momenta are calculated. The right-hand panel shows angular momentum fluxes carried by magnetic field (solid lines) and matter (dashed lines. The numbers show the regions where the angular momentum flux carried by the field is carried mostly by the closed (I), radial (II), or open (III) field lines.

through the magnetic field. In addition, we took a different structure of the disk, which is thinner and located initially at $r_d = 5$, which is closer to the star for such a strong field. We were able to model the stronger magnetic field because we increased the radius of the star (the inner boundary) to $R_* = 0.5$ (versus $R_* = 0.35$ in other simulation runs). In addition, we were able to use a grid $N_R \times N_\theta = 91 \times 31$ which speeded up the simulations and allowed longer runs, up to 1000 P_0.

For this case, we also performed a set of simulations for different corotation radii and found the state which gives torqueless accretion, $\dot{L} \approx 0$. We found that this state corresponds to a corotation radius $r_{co} \approx 4.6$. Figure 7 shows the evolution of the fluxes in this case. The angular momentum flux associated with the matter is very small as in our main case. The flux due to the magnetic field, $\dot{L}_f$, varies more strongly than in the main case. This is because the coronal density is lower so that variations of the magnetic field in the corona are larger. In addition, the accretion rate $\dot{M}$ is several times larger than that for our main case, because the disk is different compared to the main case.

We analyzed the rotational equilibrium state in detail. Figure 8a shows the evolution of the disk and magnetic field in the inner part of the simulation region. We observed that the accretion disk stopped at much larger distances, $r_A \approx 3.1$, compared to our main case ($r_A \sim 1.2 - 1.3$) because of much stronger magnetic field. This radius again coincides with the $\beta = 1$ line (see the bold red line on figure 8a). We also estimated the radius r_0 derived from comparison of magnetic and matter torques. Again, we obtained similar but a somewhat larger radius, $r_0 \approx 3.2$. We observed that in type II case, the ratio $r_{co}/r_A \sim 1.4 - 1.5$. This number is slightly larger than that in the main case ($r_{co}/r_A \sim 1.3 - 1.4$) which may be connected with contribution of the inflated field lines to the negative torque.

Figure 8b shows the angular momentum fluxes carried by the field $F_B(r,\theta)$ and by the matter $F_m(r,\theta)$. One can see that the disk matter brings positive spin-up torque (right panel), while magnetic field carries both negative and positive torques (left panel). In this case a significant part of the spin-down flux is carried by the inflated and radially stretched field lines. This is different from the type I initial conditions case.

Figure 9 shows angular distribution of fluxes $F_B(r,\theta)$ and $F_m(r,\theta)$ along the spheres of different radii r from $r = 0.5$ to $r = 4.5$. One can see, that at large distances, $r = 4.5$, there is a large positive angular momentum flux carried by the matter of the disk, and there is a large negative angular momentum flux carried by the radially stretched field lines located above the disk and in the disk. Field lines above the disk are inflated field lines which connect to the disk at large radii $r > 20$. They carry both, positive matter flux, and negative spin-down flux. In this region the density is smaller than in the disk, however, the field lines are strongly wound and azimuthal velocity is large, this is why both fluxes associated with matter and the field are large in this region. The plot at $r = 3.75$ shows relative input from different sets of field lines. It shows that in the region of the closed field lines (region I) matter carries positive torque while field lines carry only small negative torque. Most of both torque is carried by the radially stretched field lines (region II), while the role of vertically inflated field lines of "magnetic tower" (region III) is very small. At even smaller radii, $r = 3, 2, 1$ and 0.5, both torques become smaller, like in type I case.

5. EQUILIBRIUM STATE IN APPLICATIONS TO DIFFERENT STARS

The rotational equilibrium state is expected to be the most probable state for different disk accreting magnetized stars. These include Classical T Tauri Stars, cataclysimic variables, and X-ray pulsars. For example, the slowly rotating CTTSs have spin rates as low as $\sim 10\%$ of breakup speed (Bouvier et al. 1993). The fact that CTTSs rotate slowly strongly suggests that they are in rotational equilibrium state.

Below we estimate periods of rotation for different weakly magnetized stars. Our simulations were performed for cases $r_A/R_* = 4 - 6$ and can be applied to systems with different scales in which this ratio is satisfied. Observations show that in CTTS this ratio is in the range $r_A/R_* = 4{-}8$ (Bouvier et. al., 1993, Edwards et al., 1993), or, $r_A/R_* = 3 - 10$ (Kenyon, Yi & Hartmann, 1996). Similar or smaller magnetospheres are expected in accreting millisecond pulsars (van der Klis 2000) and dwarf novae cataclysmic variables (Warner 2004).

For our example we take $r_A/R_* = 4$, take obtained from simulation ratio $r_{co} = 1.4 r_A$ and derive the angular velocity for rotational equilibrium, Ω_{eq}:

$$\frac{\Omega_{eq}}{\Omega_{*K}} = \left(\frac{R_*}{r_{co}}\right)^{3/2} \approx 0.09 \ , \qquad (11)$$

which is about $\sim 10\%$ of breakup speed of the star. Here, Ω_{*K} is the Keplerian angular speed at R_*. The value of Ω_{eq}/Ω_{*K} we find is close to the one observed in CTTSs.

5.1. *Classical T Tauri Stars (CTTSs)*

The angular velocity of the star can be written as $\Omega_* = (GM/r_{co}^3)^{1/2}$. Combining this with the rotational equilibrium condition $r_{co}/r_A \sim 1.3 - 1.5$ (an average 1.4 was taken here) and using Eqn. 1 for the Alfvén radius, we can get the critical value of angular velocity Ω_{eq} or rotation period $P_{eq} = 2\pi/\Omega_{eq}$. For the CTTS we obtain the equilibrium rotation period,

$$P_{eq} \approx 4.6 \text{ days} \Big(\frac{0.8 M_\odot}{M}\Big)^{5/7} \Big(\frac{10^{-7} M_\odot/\text{yr}}{\dot{M}}\Big)^{3/7} \times \Big(\frac{B}{10^3 \text{G}}\Big)^{6/7} \Big(\frac{R_*}{2R_\odot}\Big)^{18/7}, \qquad (12)$$

where B is the surface magnetic field of the star. Our result is in the range of an observational bimodal distribution of rotation at period with peaks near 3 and 8 days (Attridge & Herbst 1992). Edwards et al. (1993) proposed that the distribution near 8 days may be caused by the disk locking. We should note that both peaks may be connected with the disk locking, but at different parameters, say, $\dot{M}$ and B.

5.2. *Cataclysmic Variables*

We next consider dwarf novae which belong to a subtype of the cataclysmic variables where the magnetic field

is expected to be small but still possibly dynamically important for the accretion. The accretion disks are stopped at small radii by the white dwarf magnetosphere. The accreting material then leaves the disk and follows the magnetic field lines down to the star's surface in the vicinity of the magnetic poles. Taking typical values for the white dwarf and accretion disk, we obtain the period of these stars in rotational equilibrium state,

$$P_{eq} \approx 57 \text{ s} \Big(\frac{M_\odot}{M}\Big)^{5/7} \Big(\frac{10^{-8} M_\odot/\text{yr}}{\dot{M}}\Big)^{3/7} \times \Big(\frac{B}{10^5 \text{G}}\Big)^{6/7} \Big(\frac{R}{7.0\times 10^8 \text{cm}}\Big)^{18/7}. \quad (13)$$

The observed periods of Dwarf Novae Oscillations (DNOs) are in the range of $7-70$ s (Warner, 2004).

5.3. *Millisecond Pulsars*

Our simulations are also applicable to millisecond X-ray pulsars, which are the accreting low-magnetic-field neutron stars (van der Klis, 2000). The period of such a star in the rotational equilibrium is

$$P_{eq} \approx 1.8 \text{ ms} \Big(\frac{1.4 M_\odot}{M}\Big)^{5/7} \Big(\frac{10^{-9} M_\odot/\text{yr}}{\dot{M}}\Big)^{3/7} \times \Big(\frac{B}{10^8 \text{G}}\Big)^{6/7} \Big(\frac{R}{10^6 \text{cm}}\Big)^{18/7}. \quad (14)$$

For all accretion-powered millisecond X-ray pulsars we have known, the spin frequencies range from 185Hz to 435Hz (Wijnands, R. 2004), or, the spin rate is in range of 2.3-5.2 ms. These values may be obtained from Eqn.14 at smallere $\dot{M}$ or larger B.

6. DISCUSSION

We investigated the conditions for the rotational equilibrium or"torqueless" accretion state using axisymmetric MHD simulations. In such a state the total angular momentum flux to the star is approximately zero. We found the equilibrium states by gradually changing the angular velocity of the star with the other parameters fixed. We considered two main cases: One with relatively low magnetic field and dense corona and second with much stronger field and lower density corona. We observed that in both cases the rotation of the star is approximately locked to the rotation of the inner radius of the disk such that a star rotates somewhat slower than the inner radius of the disk. In the first case the ratio between corotation radius of the star and the Alfvén radius r_A (where the disk is disrupted) is $r_{co}/r_A \sim 1.3-1.4$. In the second case, where stronger inflation of the magnetic field was observed, this ratio is only slightly larger, $r_{co}/r_A \sim 1.4-1.5$. We observed that in the first case, the angular momentum transport is associated with the closed field lines at the inner radii of the disk. Open field lines spin down the star, but the role of this spin-down is small. In the second case outflow of angular momentum along the inflated field lines is more significant than in the first case, however this did not change the result, which probably means that the angular momentum transport associated with the inner regions of the disk and the region of the funnel flow is more significant. Thus, in both cases the magnetic interaction effectively locks the rotation rate of the star to a value which depends mainly on the mass accretion rate and the star's magnetic moment. We should note that most of coronal region is still matter dominated. This is connected with the fact that the magnetic energy-density of the dipole decreases with distance as $\sim R^{-6}$ so that it is difficult to set up a magnetically dominated corona. Goodson et al. (1997, 1999) were able to model such a corona by arranging fast fall-off of coronal density with the distance. However, their initial conditions are sufficiently far from equilibrium that the torqueless accretion was not established. Future simulations with even lower coronal densities will help to understand whether a star is always locked to the rotation rate of the inner radius of the disk. Our simulations for two very different initial conditions have shown very similar results for the rotational equilibrium which may be a sign that the disk-locking may be a similar for all slowly rotating stars.

We applied our simulation results to Classical T Tauri stars, where disk locking may explain their slow rotation. Also, we estimated the probable periods of rotation of other accretion powered systems, such as dwarf novae and X-ray millisecond pulsars.

The authors thank Drs. Koldoba and Ustyugova for developing of codes and helpful discussions. This work was supported in part by NASA grants NAG 5-13220, NAG 5-13060 and by NSF grant AST-0307817.

REFERENCES

Agapitou, V., & Papaloizou, J. C. B. 2000, MNRAS, 317, 273
Attridge, J. M., & Herbst, W. 1992, ApJ, 398, L61
Bardou, A. 1999, MNRAS, 306, 669
Bouvier, J.Cabrit, S.,Fernández, M., Martín, E.L., & Matthews, J. M. 1993, A&A, 272,176
Bildsten, L., et al. 1997, ApJS, 113, 367
Camenzind, M. 1990, Rev. Mod. Astron., 3, 234
Davidson, K., & Ostriker, J. P. 1973, ApJ, 179, 585
Edwards, S., et al. 1993, AJ, 106, 372
Elsner, R. F., and Lamb, F. K. 1977, ApJ, 215, 897
Fendt, C., & Elstner, D. 1999, A&A, 349, L61
Ghosh, P., & Lamb, F. K. 1978, ApJ, 223, L83
Ghosh, P., Lamb, F. K. 1979, ApJ, 234, 296
Ghosh, P., Lamb, F. K., & Pethick, C. J. 1977, ApJ, 217, 578
Goodson, A. P., Böhm, K. H., & Winglee, R. 1999, ApJ, 524, 142
Goodson, A. P., Winglee, R., & Böhm, K. H. 1997, ApJ, 489, 199
Hayashi, M. R., Shibata, K., & Matsumoto, R. 1996, ApJ, 468, L37
Hirose, S., Uchida, Y., Shibata, K., & Matsumoto, R. 1997, PASJ, 49, 193
Kato, Y., Hayashi, M. R., & Matsumoto, R. 2004, ApJ, 600, 338
Kenyon, S. J., Yi, I. & Hartmann, L. 1996, ApJ, 462,439
Koldoba, A. V., Kuznetzov, O. A., & Ustyugova, G. V. 1992, Rep. Keldysh Inst. Applied Mathematics, Russian Acad. Sci., No. 69
Koldoba, A. V., Lovelace, R. V. E., Ustyugova, G. V., & Romanova, M. M. 2002, AJ, 123, 2019
Koldoba, A. V., & Ustyugova, G. V. 1994, Rep. Keldysh Inst. Applied Mathematics, Russian Acad. Sci., No. 87
Königl, A. 1991, ApJ, 370, L39
Lamb, F. K., Pethick, C. J., & Pines, D. 1973, ApJ, 184, 271
Li, J., & Wickramasinghe, D. T. 1997, MNRAS, 286, L25
Lovelace, R. V. E., Romanova, M. M., & Bisnovatyi-Kogan, G. S. 1995, MNRAS, 275, 244
Matt, S., & Pudritz, R .E. 2004, ApJ, 607, L43
Matt, S., & Pudritz, R .E. 2005, MNRAS, 356, 167
Miller, K. A., & Stone, J. M. 1997, ApJ, 489, 890
Nagase, F. 1989, PASJ, 41, 1
Pringle, J. E., & Rees, M. J. 1972, A&A, 21, 1
Romanova, M. M., Ustyugova, G. V., Koldoba, A. V., Chechetkin, V. M., & Lovelace, R. V. E. 1998, ApJ, 500, 703

Romanova, M. M., Ustyugova, G. V., Koldoba, A. V., & Lovelace, R. V. E. 2002, ApJ, 578, 420
Romanova, M. M., Ustyugova, G. V., Koldoba, A. V., & Lovelace, R. V. E. 2004, ApJ, 616, L151
Shakura, N. I., & Sunyaev, R. A. 1973, A&A, 24, 337
Shu, F. H., Najita, J., Ruden, S. P., & Lizano, S. 1994, ApJ, 429, 797
Ustyugova, G. V., Koldoba, A. V., Romanova, M. M., Chechetkin, V. M., & Lovelace, R. V. E. 1995, ApJ, 439, L39
———. 1999, ApJ, 516, 221
Uzdensky, D.A., Königl, A., & Litwin, C. 2002, ApJ, 565, 1191
van der Klis, M. 2000, Annu. Rev. Astron. Astrophys, 38, 717
Von Rekowski, B. & Brandenburg, A. 2004, A&A, 420, 17
Wang, Y.-M. 1995, ApJ, 449, L153
Warner, B. 1995, Cataclysmic Variable Stars (Cambridge: Cambridge Univ. Press)
Warner, B. 2004, PASP, 116, 115
Wijnands R., 2004, in Kaaret P., Lamb F. K., Swank J. H., eds, AIP Conf. Proc. Vol. 714, X-ray Timing 2003: Rossi and Beyond. Am. Inst. Phys., Melville, NY, p. 209

Draft version February 5, 2008
Preprint typeset using LaTeX style emulateapj v. 11/12/01

LOCKING OF THE ROTATION OF DISK ACCRETING MAGNETIZED STARS

M. Long, M.M. Romanova, R.V.E Lovelace
Department of Astronomy, Cornell University, Ithaca, NY 14853
Email: Long@astro.cornell.edu
Draft version February 5, 2008

ABSTRACT

We investigate the rotational equilibrium state of a disk accreting magnetized stars using axisymmetric magnetohydrodynamic (MHD) simulations. In this "locked" state, the spin-up torque balances the spin-down torque so that the net average torque on the star is zero. We investigated two types of initial conditions, one with a relatively weak stellar magnetic field and a high coronal density, and the other with a stronger stellar field and a lower coronal density. We observed that for both initial conditions the rotation of the star is locked to the rotation of the disk. In the second case, the radial field lines carry significant angular momentum out of the star. However, this did not appreciably change the condition for locking of the rotation of the star. We find that in the equilibrium state the corotation radius r_{co} is related to the magnetospheric radius r_A as $r_{co}/r_A \approx 1.2-1.3$ for case (1) and $r_{co}/r_A \approx 1.4-1.5$ for case (2). We estimated periods of rotation in the equilibrium state for classical T Tauri stars, dwarf novae and X-ray millisecond pulsars.

Subject headings: accretion, accretion disks - magnetic fields - plasma - stars: magnetic fields

1. INTRODUCTION

Disk accretion to a rotating star with a dipole magnetic field is important in a number of astrophysical objects, including T Tauri stars (Camenzind 1990; Königl 1991), X-ray pulsars (Nagase 1989; Bildsten et al. 1997), and cataclysmic variables (Warner 1995). An important property of this interaction is the disruption of the disk at the Alfvén radius, r_A, and the "locking" of the star's angular rotation at an angular velocity, Ω_{eq}, which is expected to be of the order of the disk rotation rate at the Alfvén radius, $\Omega(r_A) = (GM/r_A^3)^{1/2}$. However, the exact conditions for locking and for the value of the equilibrium rotation rate Ω_{eq} (when the star does not spin up or spin down) were not been established.

One of the complicated aspects of the disk-magnetosphere interaction is the process of angular momentum transport between the disk and the magnetized star. In the first models of the disk-magnetosphere interaction it was proposed that the magnetic field has a dipole configuration everywhere and that the net change between spin-up torque which arises from the magnetic connection of the star to the disk within the corotation radius r_{co} and the spin-down torque which arises from the connection beyond the corotation radius determines the spin evolution of the star (Ghosh, Lamb & Pethick 1977; Ghosh & Lamb 1978, 1979 - hereafter GL79). The corotation radius is the radius where the disk rotates at the same speed as a star, $r_{co} = (GM/\Omega_*^2)^{1/3}$. It was suggested that for a particular value of the star's rotation rate, Ω_{eq}, the positive spin-up torque balances the negative spin-down torque and the star is in the rotational equilibrium state (Ghosh & Lamb 1978, 1979; Wang 1995).

Recent studies of the evolution of the magnetic field threading the disk and the star led to understanding that the field tends to be inflated and possibly opened due to the difference in the angular velocities of the foot-points (Lovelace, Romanova & Bisnovatyi-Kogan 1995 - hereafter LRBK; Shu et al. 1994; Bardou 1999, Uzdensky, Königl & Litwin 2002). In this case a star may lose some angular momentum through the open field lines and the equilibrium state will be determined by the balance between processes of spin-up/spin-down associated with the disk-magnetosphere interaction, and spin-down associated with the open field lines.

In some models it was suggested that the angular momentum transport between the star and the disk may be much less efficient (Agapitou & Papaloizou 2000) if the field lines are opened as proposed by LRBK. Under such conditions the rotational equilibrium state will be quite different (e.g., Matt & Pudritz 2004, 2005). The goal of this paper is to derive the conditions for the rotational equilibrium state using axisymmetric MHD simulations of the disk-magnetosphere interaction.

The properties of the rotational equilibrium state depend on the configuration of the magnetic field threading the star and the disk. Consequently, analysis of this problem requires two or three dimensional simulations. Axisymmetric simulations have shown that the field lines do open (Hayashi et al. 1996; Miller & Stone 1997; Hirose et al. 1997; Romanova et al. 1998; Fendt & Elstner 1999). However, longer runs have shown that the innermost field lines reconnect to form a closed magnetosphere, and some of them open and close again in a recurrent manner (Goodson & Winglee 1997; Goodson, Winglee & Böhm 1999; Romanova et al. 2002, hereafter RUKL; Romanova et al. 2004; Kato et al. 2004, Von Rekowski & Brandenburg 2004). Detailed simulations of the slow, viscous disk accretion to a rotating star with an aligned dipole field (RUKL) have shown that on long time-scales, the magnetic field lines in the vicinity of the Alfvén radius r_A are closed or only partially open, and these lines are important for the angular momentum transport between the star and the disk. The balance between the magnetic flux in closed and open field lines is clearly important for determining the rotational equilibrium state.

In RUKL, a preliminary search for the conditions of

torqueless accretion was performed and the torqueless accretion was shown to exist. In this paper, we give a detailed study of the conditions for torqueless accretion using an improved axisymmetric MHD code which makes possible longer simulation runs compared to RUKL. The main question is: What is the angular rotation rate of a star Ω_{eq} for the torqueless accretion given the star's mass M, magnetic moment μ, and accretion rate $\dot{M}$. Equivalently, if we know the Alfvén radius r_A, then what is the corotation radius r_{co} in the rotational equilibrium state? In earlier theoretical models, it was estimated that the critical fastness parameter $\omega_s = \Omega_*/\Omega_K(r_A) = (r_A/r_{co})^{3/2}$ of the equilibrium state is in the range of $0.47 - 0.95$ (Li & Wickramasinghe 1997). This corresponds to the ratio $r_{co}/r_A \sim 1.1 - 1.7$.

In this paper we determine the value of r_{co}/r_A for torqueless accretion numerically by performing a large set of numerical simulations for different values of Ω_*, μ, $\dot{M}$, and disk/corona parameters. We also investigated the matter flow and the angular momentum transport in the equilibrium state. In §2, the numerical model is described. We focus on conditions where the torqueless accretion occurs and study its dependence on different physical parameters for different cases in §3 and 4. In §5, we apply our results to relevant objects, such as CTTSs, cataclysmic variables, and X-ray millisecond pulsars. We discuss results in Section 6.

2. THEORETICAL IDEAS AND NUMERICAL SIMULATIONS

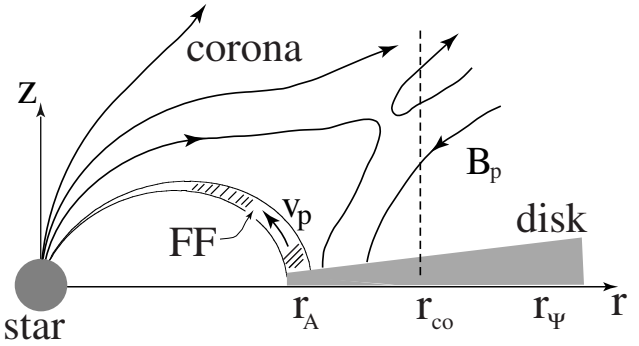

FIG. 1.— Sketch of disk accretion to a star with an aligned dipole magnetic field, where r_A is the Alfvén radius, r_{co} is corotation radius, r_Ψ is the deviation radius where a significant deviation from Keplerian rotation occurs for $r < r_\Psi$ due to the magnetic force on the disk. The dashed line divides the rapidly rotating region and the slowly rotating region. FF denotes the funnel flow.

Theoretical aspects of the disk-magnetoshpere interaction were developed in the 1970s (e.g. Pringle & Rees, 1972; Ghosh, Lamb & Pethick 1977; GL79). As sketched in Figure 1, the initial Keplerian accretion disk is threaded by the star's magnetic field. The inner radius of the disk, referred to as the Alfvén radius r_A, occurs at the radial distance where the energy-density of matter in the disk equals to magnetic energy-density, or where the paramter $\beta = \rho v^2/(B^2/8\pi) = 1$. (e.g., Lamb, Pethick & Pines 1973; Davidson & Ostriker 1973). We observed from many simulations that the inner radius of the disk coincides with this radius. The Alfvén radius is usually derived analytically using a number of approximations. For a dipole magnetic field of the star, $\mu \equiv B_* R_*^3 = B r^3$,

$$r_A = k_A r_A^{(0)} = k_A \frac{\mu^{4/7}}{(2GM)^{1/7}\dot{M}^{2/7}} \ . \quad (1)$$

Here, G is the gravitational constant, $\dot{M}$ is the mass accretion rate, M is the mass of the star, $r_A^{(0)}$ is the Alfvén radius for the spherical accretion (Elsner & Lamb 1977). The coefficient k_A accounts for the fact that the disk accretion is different from spherical accretion. Using values of the different parameters obtained from our simulations we obtained $r_A^{(0)}$ and then compared it with r_A. From this we obtained $k_A \approx 0.5$.

In a somewhat different approach, Wang (1995) suggested that the disk stops or disrupts at the radius r_0 where the magnetic and matter stresses are equal, $(-r^2 B_\phi B_z)_0 = \dot{M}[\mathrm{d}(r^2\Omega)/\mathrm{d}r]_0$, where the 0−subscripts indicate evaluation at $r = r_0$, B_ϕ and B_z are the components of the magnetic field, Ω is the angular velocity of the disk. We took values of parameters from our simulations and derived the radius the radius r_0. We observed that this radius approximately coincides with r_A.

Whether a star spins up or spins down is due to angular momentum flow to or out of the star transported by the matter flow and the magnetic field. Some field lines of the star thread the disk and transport angular momentum between the disk and the star (e.g., GL79). Other field lines are inflated and become open, that is, not connected to the disk. These open field lines may transport angular momentum away from the star to the corona without direct interaction with the disk (Agapitou & Papaloizou 2000; Matt & Pudritz 2004). We observed that both closed and open field lines contribute to the angular momentum transport to the star.

For the case where the poloidal field lines connect the star and the disk, the field lines passing through the disk within the corotation radius r_{co} spin up the star, while the field lines passing through the disk at large distances spin it down (GL79). The dashed vertical line in Figure 1 at r_{co} divides the regions which provide positive and negative torques. There is also a region $r \lesssim r_\Psi$ where the magnetic interaction modifies the Keplerian rotation of the disk, and where the angular momentum transport between the star and the disk is important (GL79, RUKL). If some of the magnetic field lines are open, then angular momentum may be also transported outward from the disk and from the star through twisting of open magnetic field lines. Thus part of the angular momentum flux may be transported by the matter flow, part by the open field lines, and part by closed field lines connecting the star and the disk.

2.1. *Main Equations*

The disk-magnetoshpere interaction is considered to be described by the MHD equations,

$$\frac{\partial \rho}{\partial t} + \nabla \cdot (\rho \mathbf{v}) = 0 \ , \quad (2)$$

$$\rho \frac{\mathrm{d}\mathbf{v}}{\mathrm{d}t} = -\nabla p + \rho\, \mathbf{g} + \frac{1}{4\pi}(\nabla \times \mathbf{B}) \times \mathbf{B} + \mathbf{F}^{vis} \ , \quad (3)$$

$$\frac{\partial \mathbf{B}}{\partial t} = \nabla \times (\mathbf{v} \times \mathbf{B}) \ , \quad (4)$$

$$\frac{\partial (\rho S)}{\partial t} + \nabla \cdot (\rho \mathbf{v} S) = 0 \ , \quad (5)$$

$$\nabla \cdot \mathbf{B} = 0 \ . \tag{6}$$

Here, $S = p/\rho^\gamma$ is the entropy per gram, $\mathbf{g}$ is the gravitational acceleration, $\mathbf{F}^{vis}$ is the viscous force. The viscosity model of Shakura and Sunyaev (1973) is used with viscosity coefficient $\nu = \alpha c_s^2/\Omega_K$, where $c_s = (\gamma p/\rho)^{1/2}$ is the sound speed, and parameter α is dimensionless with values $\alpha \sim 0.01 - 0.03$ considered here.

Equations 2-6 were solved with a Godunov-type numerical code developed by Koldoba, Kuznetzov & Ustyugova (1992) (see also Koldoba & Ustyugova 1994; Ustyugova et al. 1995). We used an axisymmetric spherical coordinates with a grid $N_r \times N_\theta = 131 \times 51$. Test simulations with larger or smaller grids were also performed.

2.2. *Reference Units*

We let R_0 denote a reference distance scale, which is equal to $R_*/0.35$ where R_* is the radius of the star. The subscript "0" denotes reference values for units. We take the reference value for the velocity, $v_0 = (GM/R_0)^{1/2}$, the angular speed $\Omega_0 = v_0/R_0$, the timescale $P_0 = 2\pi R_0/v_0$, the magnetic field $B_0 = B_*(R_*/R_0)^3$, the magnetic moment $\mu_0 = B_0 R_0^3$, the density $\rho_0 = B_0^2/v_0^2$, the pressure $p_0 = \rho_0 v_0^2$, the mass accretion rate $\dot{M}_0 = \rho_0 v_0 R_0^2$, and the angular momentum flux $\dot{L}_0 = \rho_0 v_0^2 R_0^3$. The dimensionless variables are $\widetilde{R} = R/R_0$, $\widetilde{v} = v/v_0$, $\widetilde{T} = T/P_0$ etc. In the following we use these dimensionless units but the tildes are implicit.

2.3. *Boundary and Initial Conditions*

Boundary conditions: At the inner boundary $R = R_*$, "free" boundary conditions are applied for the density, pressure, entropy, velocity, and $\phi-$component of the magnetic field, $\partial\rho/\partial R = 0$, $\partial p/\partial R = 0$, $\partial S/\partial R = 0$, $\partial(\mathbf{v} - \mathbf{\Omega} \times \mathbf{R})_R/\partial R = 0$, $\partial(RB_\phi)/\partial R = 0$. The poloidal components B_R and B_θ are derived from the magnetic flux function $\Psi(R, \theta)$, where Ψ at the boundary is derived from the frozen-in condition $\partial\Psi/\partial t + \mathbf{v}_p \cdot \nabla\Psi = 0$. At the outer boundary, free boundary conditions are taken for all variables. The outer boundary was placed far away from the star in order to diminish the possible influence of this boundary (Ustyugova et al. 1999).

Initial conditions: The star has a fixed aligned dipole magnetic field with magnetic moment μ. The initial accretion disk extends inward to an inner radius r_d, and it has a temperature T_d which is much less than the temperature of the corona T_c. The initial disk and corona are in pressure balance. The corona above the disk rotates with the angular velocity of the disk in order to avoid a rapid initial shearing of the magnetic field. The initial density distributions in the disk and corona are constrained by the condition that there is a balance of pressure gradient, gravitational and centrifuge forces. This balance is necessary in order to have smooth accretion flow which evolves on the viscous time scale of the disk (see details in RUKL). To avoid a very strong initial interaction of the disk with the magnetic field, we take the initial inner radius of the disk at $r_d = 6$ or $r_d = 5$, far away from the star.

In order to investigate the rotational equilibrium states, we performed simulations with two types of initial conditions, type I and type II. For type I initial conditions we have a magnetic field which is relatively weak, $\mu = 2$, the disk is relatively thick with fiducial density $\rho_d = 1$, and relatively high coronal density, $\rho_{cor} = 0.005$. The initial inner disk radius is $r_d = 6$. The outer radius of simulation domain corresponds to $18R_0$, that is, about $54R_*$. Results for this case are described in §3. For type II initial conditions the star's magnetic field is much stronger, $\mu = 10$, the coronal density is much lower $\rho_{cor} = 0.001$, the disk is thinner, and the initial inner disk radius is $r_d = 5$. The outer radius of simulation domain corresponds to $68R_0$, that is, about $136R_*$.These initial conditions, which are more favorable for inflation and opening of the coronal field lines, are described in §4.

3. THE EQUILIBRIUM STATE OF DISK ACCRETION FOR INITIAL CONDITIONS OF TYPE I

3.1. *Search for Rotational Equilibrium State*

Whether the star spins up or spins down is determined by the net flux of angular momentum to the surface of the star, $\dot{L}$. This flux is composed of two parts, the flux carried by the matter $\dot{L}_m$, and that carried by the magnetic field, $\dot{L}_f$:

$$\dot{L} = \dot{L}_m + \dot{L}_f \ , \tag{7}$$

$$\dot{L}_m = -\int \mathrm{d}\mathbf{S} \cdot \rho r v_\phi \mathbf{v}_p \ , \tag{8}$$

$$\dot{L}_f = \frac{1}{4\pi} \int \mathrm{d}\mathbf{S} \cdot r B_\phi \mathbf{B}_p \ , \tag{9}$$

where the $p-$subscript denotes the poloidal component, and $\mathrm{d}\mathbf{S}$ is the outward pointing surface area element of the star. We performed a set of simulations for different angular velocities of the star, Ω_*, to find the critical value of Ω_*, corresponding to the rotational equilibrium state, that is, the state when $\dot{L} \approx 0$. Other parameters $(\dot{M}, \mu)$ were fixed.

We observed that $\dot{L}_f$ is always dominant over $\dot{L}_m$ for all cases (as in RUKL) and thus we compared $\dot{L}_f$ for these cases. This was predicted in earlier theoretical research (e.g., GL79). We narrowed the set of Ω_* values so that $\dot{L}_B$ was very small on average (see Figure 2a). Among these we picked the one for which $\dot{L}_f \approx 0$ that corresponds to the rotational equilibrium state, $\Omega_* = \Omega_{eq}$. For this case, the corotation radius $(r_{co})_{eq} \approx 1.7$.

In addition, we calculated matter flux to the star,

$$\dot{M} = -\int \mathrm{d}\mathbf{S} \cdot \rho \mathbf{v}_p. \tag{10}$$

Figure 2b shows the mentioned fluxes in the rotational equilibrium state. Note that this state is typically reached at $T > 50$ because initially the disk is far from the magnetosphere and it takes time for the disk to move inward. One can see that the angular momentum flux carried by the field $\dot{L}_f$ fluctuates around zero.

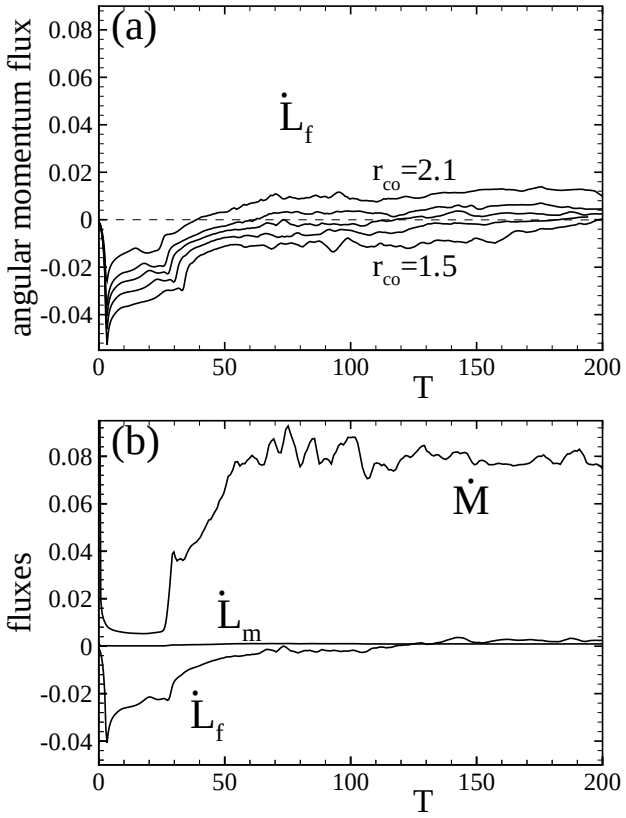

FIG. 2.— (a) The evolution of $\dot{L}_f$ for different corotation radii from $r_{co} = 1.5$ (bottom line) to $r_{co} = 2.1$ (top line); (b) The evolution of $\dot{M}$ and the angular momentum fluxes carried by matter $\dot{L}_m$ and the magnetic field $\dot{L}_f$ in rotational equilibrium state, $r_{co} \approx 1.7$. Time scale is P_0 (see §2.2).

3.2. *Disk-Magnetosphere Interaction in Equilibrium State*

We now discuss in more detail the rotational equilibrium state where $r_{co} = 1.7$. Figure 3a shows the evolution of matter and the magnetic flux with time. One can see that initially the disk matter moves inward, then it stops near magnetosphere and goes to the star through a funnel flow which is driven up by pressure gradient force (RUKL;Koldoba et al. 2002). The funnel flow is quasi-stationary after a time $T \sim 50$. The bold red line divides the regions where magnetic and matter energy densities dominate, that is, the line where $\beta = 1$ (see §2). The corresponding Alfvén radius is $r_A \approx 1.2 - 1.3$. We also estimated the radius r_0 derived from the equality of magnetic and matter stresses. We observed that this radius is close to r_A, $r_0 \approx 1.3 - 1.4$.

Figure 3a shows that the magnetic field for $r > r_A$ is strongly non-dipolar, and the structure of the field is complicated. The magnetic field lines initially inflate for $T < 30$; however, later some of them reconnect forming closed field lines and thus enhancing the dipole component in the closed magnetosphere. Other field lines, which are near the axis stay open and represent the lines of "magnetic tower", which is often observed in different simulations of the disk-magnetosphere interaction (e.g., Kato et al. 2004; Romanova et al. 2004). Many field lines are radially stretched by the accreting matter. These field lines are located in the disk and above the disk. Most of these field lines are connected to the star. The field lines above the closed magnetosphere continue to open and reconnect in quasi-periodic manner. In case of the lower density corona (see §4), inflation is more efficient, and this leads to larger quasi-periodic oscillations of the magnetic flux and associated fluxes.

We analyzed the angular momentum transport between the star and the disk and corona. Figure 3b shows the distribution of the angular momentum fluxes carried by the field $\mathbf{f}_B = rB_\phi \mathbf{B}_p/4\pi$ (left panel) and carried by the matter $\mathbf{f}_m = -\rho r v_\phi \mathbf{v}_p$ (right panel). One can see that for $r > r_A$, most of the angular momentum flux is carried by the matter (see the region with the high positive angular momentum at the right panel). However, for $r \lesssim r_A$ it is mainly transported by the magnetic field (see left panel of Figure 3b). The streamlines in the Figure 3b show direction of the flow of angular momentum. One can see that matter always carries positive angular momentum towards the star, which tends to spin up the star. Magnetic field lines carry angular momentum out of the star through the field lines threading the area of the funnel flow and corona. The situation with the angular momentum transport seems to be more complicated compared to one described by GL79.

The angular momentum fluxes change with distance and with angle. We calculated the angular distribution of fluxes $F_B(r,\theta) = 2\pi r^2 \sin\theta \mathbf{f}_B \cdot \hat{r}$ and $F_m(r,\theta) = 2\pi r^2 \sin\theta \mathbf{f}_m \cdot \hat{r}$ through the spheres of different radii r. Figure 4 shows that at a large radius, $r = 1.8$, matter carries most of the angular momentum, while the magnetic field also contributes but with the opposite sign. At smaller radii, the fluxes become smaller and the largest flux is in the region of the funnel flow. At the surface of the star, the flux associated with matter is very small. The flux associated with the field has two components of the opposite sign which cancel each other approximately.

The distribution of angular momentum flux is more complicated compared to that of theoretical models. However, the equilibrium state does exist and the ratio r_{co}/r_A is not very much larger than unity. This means that the rotation of the star is efficiently locked to the rotation of the inner regions of the disk.

One can see from Figure 3a, that a significant part of the disk is disturbed by the disk-magnetosphere interaction. Figure 5 shows the distribution of the angular velocity of the disk in the equatorial plane. We observed that the angular velocity varies around the Keplerian value and is usually slightly smaller then Keplerian. The magnetic field is strongly wound up in the disk so that the azimuthal field dominates. The inner regions of the disk $r \lesssim r_\Psi \sim 4$ are appreciably influenced by the magnetic field.

3.3. *Dependence on μ and α*

Next, we took a star in the rotational equilibrium state ($r_{co} = 1.7$) and varied the magnetic moment of the star μ. Figure 6a shows that when μ increases, the rate of change of angular momentum of the star becomes more negative, that is a star spins-down. This is connected with the fact that for larger μ, the magnetosphere is larger and the flux of the positive angular momentum to the star is smaller than in the equilibrium state. For example, for $\mu = 4$, the inner disk radius is at $r_A \approx 1.6$. At this in-

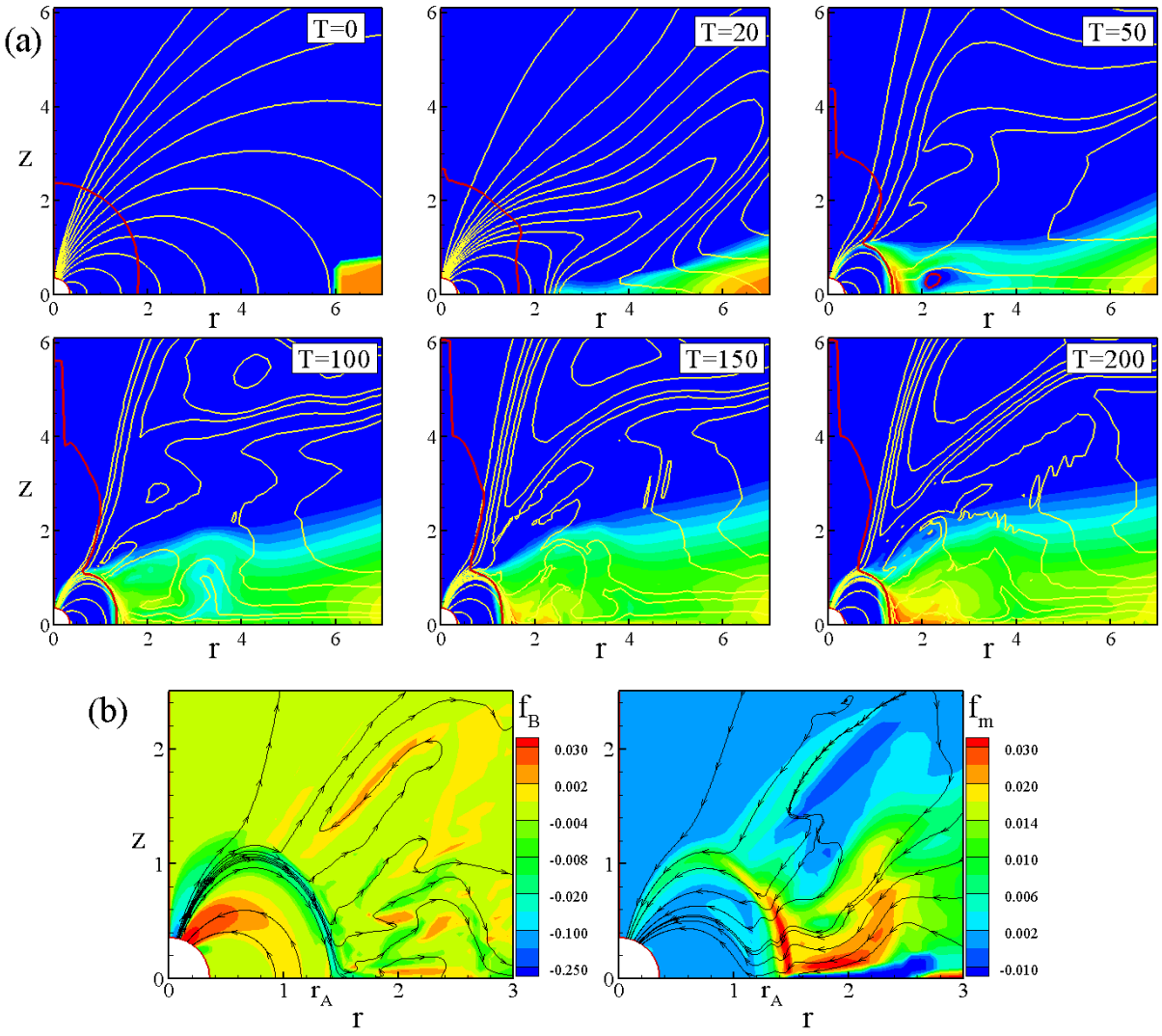

FIG. 3.— (a). Evolution of the density (color background), and the magnetic field (yellow lines) in rotational equilibrium state for type I initial conditions for $T = 0 - 200$ rotations. The density changes from $\rho = 2$ in the disk to $\rho = 0.005$ in the corona. The bold red line corresponds to $\beta = 1$ (see §2). (b). Fluxes of angular momentum carried by magnetic field $\mathbf{f}_B$ (left panel) and by matter $\mathbf{f}_m$ (right panel) at $T = 200$. Color background shows value of the fluxes, the streamlines with arrows - the direction of the angular momentum flow.

ner radius, the disk rotates much slower than the star and a star strongly spins down. Roughly, the dependence is

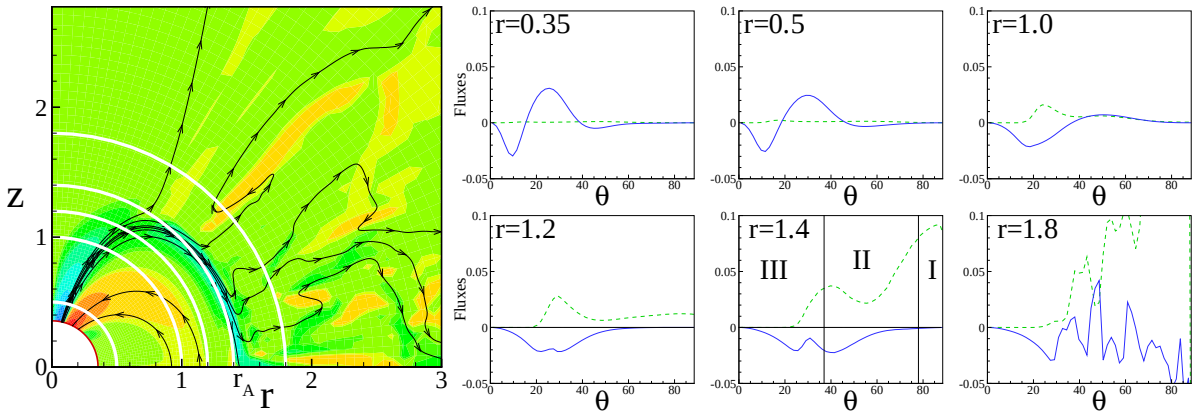

FIG. 4.— Angular distribution of fluxes $F_m(r,\theta)$ and $F_B(r,\theta)$ for type I initial conditions. The left-hand panel shows radii along which the angular momentum fluxes are calculated. The right-hand panel shows the angular momentum fluxes carried by the magnetic field (solid lines) and the matter (dashed lines) at different radii r. The numbers show the regions where the angular momentum flux carried by the field is carried mostly by the closed (I), radial (II), or open (III) field lines.

$\dot{L}_f \sim -0.02\mu + 0.04$. The balance between spin-up and spin-down torques is similar to that suggest by the GL79 model, where positive and negative torques are associated with regions within and beyond the corotation radius. We also observed different regions contributing positive and negative angular momentum fluxes. However now the distribution of the external to the Alfvén surface field lines is more complicated.

We calculated the average value of r_A for each μ and obtained the dependence $r_A \sim \mu^{\kappa}$, with $\kappa = 0.36$. This coefficient κ is somewhat different from that of equation (1) where $k = 4/7 \approx 0.57$. The difference may be connected with the fact that in the theoretical analysis the magnetic field is assumed to be a pure dipole field everywhere, whereas the simulations show that the actual field is different from a dipole for $r \gtrsim r_A$. In this and all above simulations, the viscosity coefficient was fixed at the value $\alpha = 0.02$.

We also performed simulation runs for different values of the disk viscosity, $\alpha = 0,\ 0.01,\ 0.02$, and 0.03, with other parameters fixed. We observed that for larger α the accretion rate is larger, and the Alfvén radius r_A is smaller. Thus, the region of positive torque becomes larger than the region of negative torque, and $\dot{L}_f$ is larger. In other words, at a higher accretion rate $\dot{M}$, incoming matter brings more of positive angular momentum, which is transferred to larger angular momentum flux carried by the field $\dot{L}_f$. The angular momentum flux increases with α (see Figure 6b) as about $\dot{L}_f \sim \alpha^{1.9}$ for $\alpha \geq 0.01$.

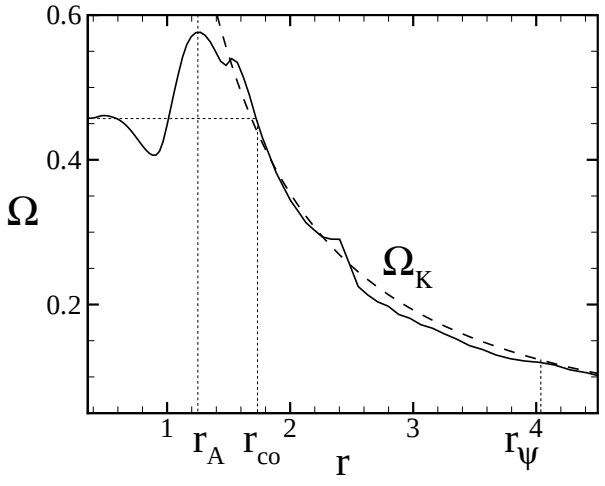

FIG. 5.— Radial distribution of angular velocity of the disk along in the equatorial plane at $T = 180$. The dash line shows Keplerian angular velocity.

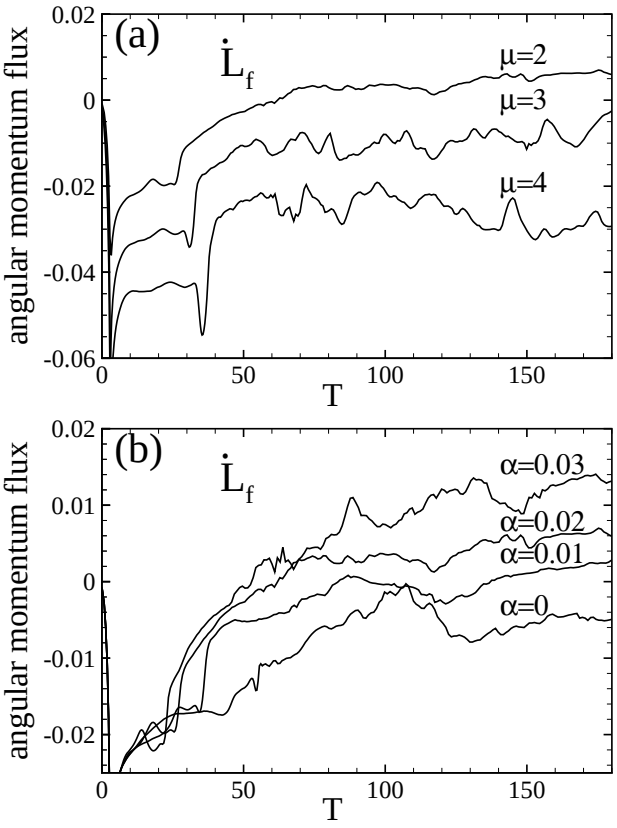

FIG. 6.— (a) The evolution of the angular momentum flux to the star carried by the magnetic field $\dot{L}_f$ for different magnetic moments of the star μ with other parameters fixed. (b) The evolution of the angular momentum flux carried by magnetic field $\dot{L}_f$ for different values of of the disk viscosity α with other parameters fixed.

4. EQUILIBRIUM STATE OF DISK ACCRETION FOR INITIAL CONDITIONS OF TYPE II

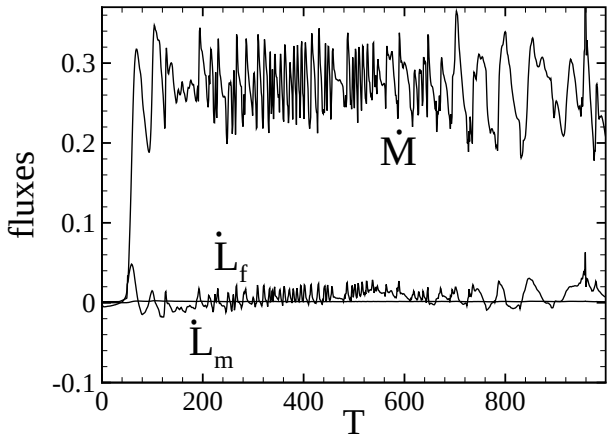

FIG. 7.— The evolution of the matter flux $\dot{M}$ and the angular momentum fluxes carried by matter $\dot{L}_m$ and magnetic field $\dot{L}_f$ in the rotational equilibrium state for the type II initial conditions.

Here we consider another case corresponding to quite different initial conditions referred to as type II. This case has a stronger magnetic field, $\mu = 10$, and a much lower coronal density, $\rho_{cor} = 0.001$. The density in the corona influences the evolution of the magnetic field in the corona, namely, the inflation and opening of the magnetic field

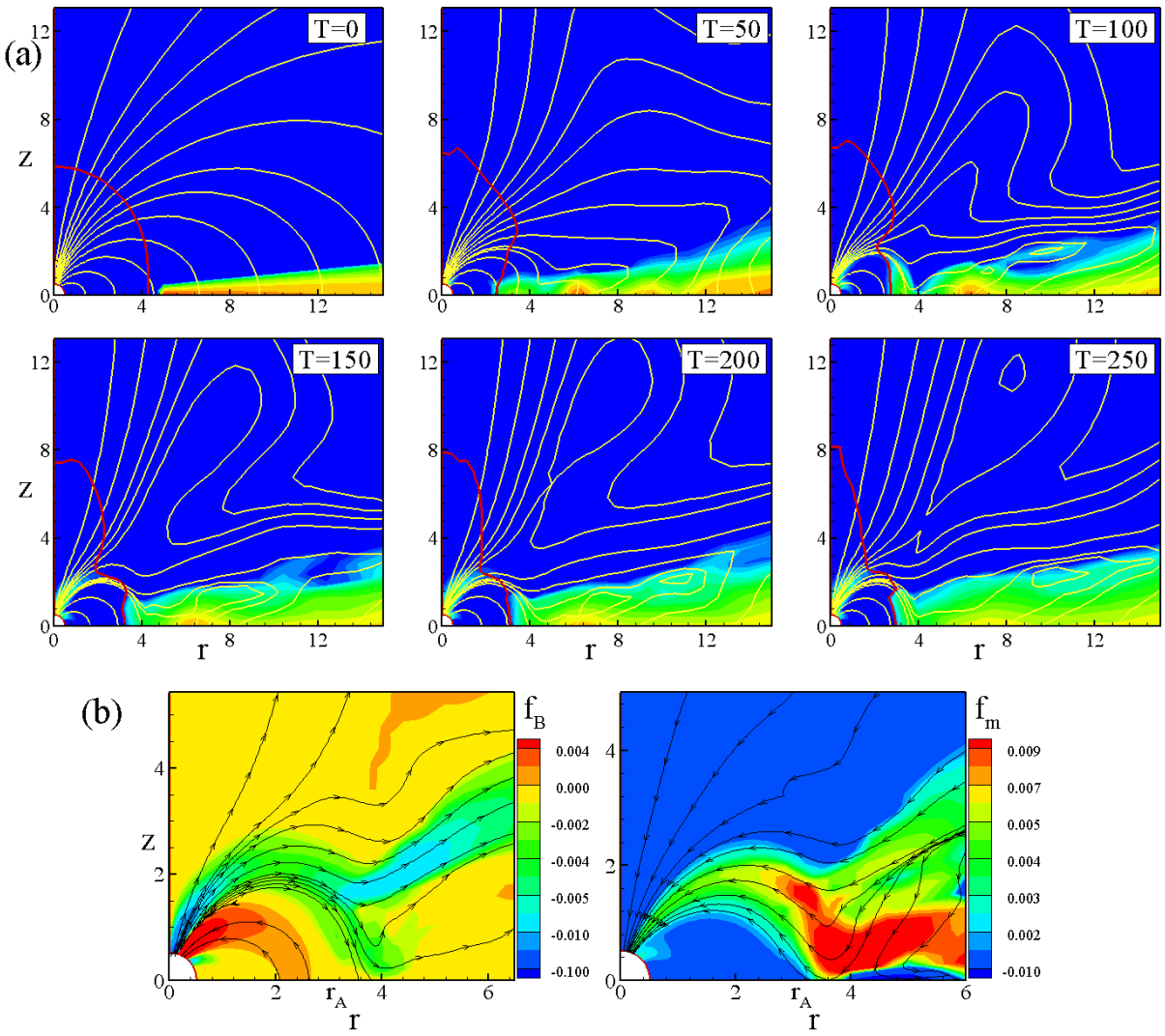

FIG. 8.— (a). Evolution of the density (color background), and the magnetic field lines (yellow lines) in rotational equilibrium state of type II initial conditions for $T = 0 - 250$ rotations. The density changes from $\rho = 2$ in the disk to $\rho = 0.001$ in the corona. The bold red line corresponds to $\beta = 1$ (see §2). (b). Fluxes of angular momentum carried by magnetic field $\mathbf{f}_B$ (left panel) and by matter $\mathbf{f}_m$ (right panel) at $T = 250$. Color background shows value of the fluxes, the streamlines with arrows - the direction of the angular momentum flow.

lines is favored. As discussed earlier, the angular momentum transport between the disk and star occurs in part

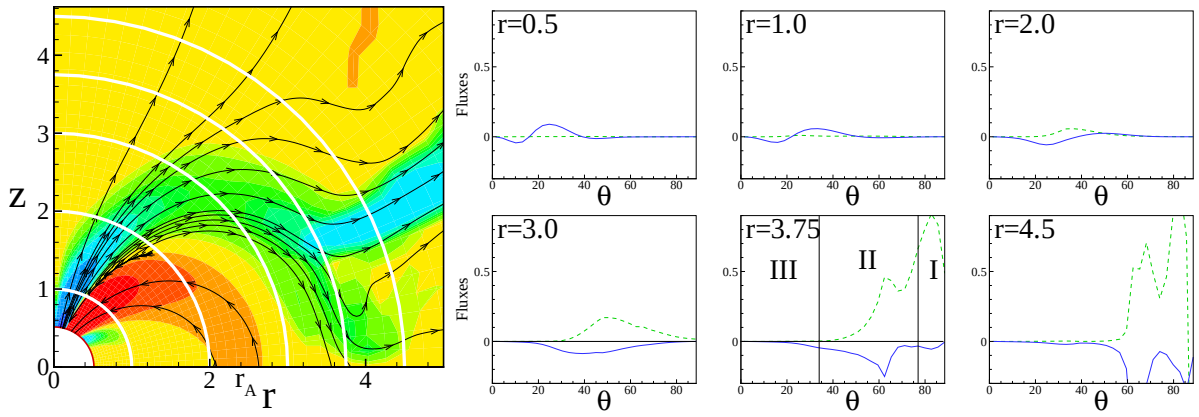

FIG. 9.— Angular distribution of fluxes $F_m(r,\theta)$ and $F_B(r,\theta)$ for initial conditions of type II. The left-hand panel shows radii along which the angular momenta are calculated. The right-hand panel shows angular momentum fluxes carried by magnetic field (solid lines) and matter (dashed lines. The numbers show the regions where the angular momentum flux carried by the field is carried mostly by the closed (I), radial (II), or open (III) field lines.

through the magnetic field. In addition, we took a different structure of the disk, which is thinner and located initially at $r_d = 5$, which is closer to the star for such a strong field. We were able to model the stronger magnetic field because we increased the radius of the star (the inner boundary) to $R_* = 0.5$ (versus $R_* = 0.35$ in other simulation runs). In addition, we were able to use a grid $N_R \times N_\theta = 91 \times 31$ which speeded up the simulations and allowed longer runs, up to 1000 P_0.

For this case, we also performed a set of simulations for different corotation radii and found the state which gives torqueless accretion, $\dot{L} \approx 0$. We found that this state corresponds to a corotation radius $r_{co} \approx 4.6$. Figure 7 shows the evolution of the fluxes in this case. The angular momentum flux associated with the matter is very small as in our main case. The flux due to the magnetic field, $\dot{L}_f$, varies more strongly than in the main case. This is because the coronal density is lower so that variations of the magnetic field in the corona are larger. In addition, the accretion rate $\dot{M}$ is several times larger than that for our main case, because the disk is different compared to the main case.

We analyzed the rotational equilibrium state in detail. Figure 8a shows the evolution of the disk and magnetic field in the inner part of the simulation region. We observed that the accretion disk stopped at much larger distances, $r_A \approx 3.1$, compared to our main case ($r_A \sim 1.2 - 1.3$) because of much stronger magnetic field. This radius again coincides with the $\beta = 1$ line (see the bold red line on figure 8a). We also estimated the radius r_0 derived from comparison of magnetic and matter torques. Again, we obtained similar but a somewhat larger radius, $r_0 \approx 3.2$. We observed that in type II case, the ratio $r_{co}/r_A \sim 1.4 - 1.5$. This number is slightly larger than that in the main case ($r_{co}/r_A \sim 1.3 - 1.4$) which may be connected with contribution of the inflated field lines to the negative torque.

Figure 8b shows the angular momentum fluxes carried by the field $F_B(r,\theta)$ and by the matter $F_m(r,\theta)$. One can see that the disk matter brings positive spin-up torque (right panel), while magnetic field carries both negative and positive torques (left panel). In this case a significant part of the spin-down flux is carried by the inflated and radially stretched field lines. This is different from the type I initial conditions case.

Figure 9 shows angular distribution of fluxes $F_B(r,\theta)$ and $F_m(r,\theta)$ along the spheres of different radii r from $r = 0.5$ to $r = 4.5$. One can see, that at large distances, $r = 4.5$, there is a large positive angular momentum flux carried by the matter of the disk, and there is a large negative angular momentum flux carried by the radially stretched field lines located above the disk and in the disk. Field lines above the disk are inflated field lines which connect to the disk at large radii $r > 20$. They carry both, positive matter flux, and negative spin-down flux. In this region the density is smaller than in the disk, however, the field lines are strongly wound and azimuthal velocity is large, this is why both fluxes associated with matter and the field are large in this region. The plot at $r = 3.75$ shows relative input from different sets of field lines. It shows that in the region of the closed field lines (region I) matter carries positive torque while field lines carry only small negative torque. Most of both torque is carried by the radially stretched field lines (region II), while the role of vertically inflated field lines of "magnetic tower" (region III) is very small. At even smaller radii, $r = 3, 2, 1$ and 0.5, both torques become smaller, like in type I case.

5. EQUILIBRIUM STATE IN APPLICATIONS TO DIFFERENT STARS

The rotational equilibrium state is expected to be the most probable state for different disk accreting magnetized stars. These include Classical T Tauri Stars, cataclysimic variables, and X-ray pulsars. For example, the slowly rotating CTTSs have spin rates as low as $\sim 10\%$ of breakup speed (Bouvier et al. 1993). The fact that CTTSs rotate slowly strongly suggests that they are in rotational equilibrium state.

Below we estimate periods of rotation for different weakly magnetized stars. Our simulations were performed for cases $r_A/R_* = 4 - 6$ and can be applied to systems with different scales in which this ratio is satisfied. Observations show that in CTTS this ratio is in the range $r_A/R_* = 4{-}8$ (Bouvier et. al., 1993, Edwards et al., 1993), or, $r_A/R_* = 3 - 10$ (Kenyon, Yi & Hartmann, 1996). Similar or smaller magnetospheres are expected in accreting millisecond pulsars (van der Klis 2000) and dwarf novae cataclysmic variables (Warner 2004).

For our example we take $r_A/R_* = 4$, take obtained from simulation ratio $r_{co} = 1.4 r_A$ and derive the angular velocity for rotational equilibrium, Ω_{eq}:

$$\frac{\Omega_{eq}}{\Omega_{*K}} = \left(\frac{R_*}{r_{co}}\right)^{3/2} \approx 0.09 \ , \qquad (11)$$

which is about $\sim 10\%$ of breakup speed of the star. Here, Ω_{*K} is the Keplerian angular speed at R_*. The value of Ω_{eq}/Ω_{*K} we find is close to the one observed in CTTSs.

5.1. *Classical T Tauri Stars (CTTSs)*

The angular velocity of the star can be written as $\Omega_* = (GM/r_{co}^3)^{1/2}$. Combining this with the rotational equilibrium condition $r_{co}/r_A \sim 1.3 - 1.5$ (an average 1.4 was taken here) and using Eqn. 1 for the Alfvén radius, we can get the critical value of angular velocity Ω_{eq} or rotation period $P_{eq} = 2\pi/\Omega_{eq}$. For the CTTS we obtain the equilibrium rotation period,

$$P_{eq} \approx 4.6 \text{ days} \Big(\frac{0.8 M_\odot}{M}\Big)^{5/7} \Big(\frac{10^{-7} M_\odot/\text{yr}}{\dot{M}}\Big)^{3/7} \times \Big(\frac{B}{10^3 \text{G}}\Big)^{6/7} \Big(\frac{R_*}{2R_\odot}\Big)^{18/7}, \qquad (12)$$

where B is the surface magnetic field of the star. Our result is in the range of an observational bimodal distribution of rotation at period with peaks near 3 and 8 days (Attridge & Herbst 1992). Edwards et al. (1993) proposed that the distribution near 8 days may be caused by the disk locking. We should note that both peaks may be connected with the disk locking, but at different parameters, say, $\dot{M}$ and B.

5.2. *Cataclysmic Variables*

We next consider dwarf novae which belong to a subtype of the cataclysmic variables where the magnetic field

is expected to be small but still possibly dynamically important for the accretion. The accretion disks are stopped at small radii by the white dwarf magnetosphere. The accreting material then leaves the disk and follows the magnetic field lines down to the star's surface in the vicinity of the magnetic poles. Taking typical values for the white dwarf and accretion disk, we obtain the period of these stars in rotational equilibrium state,

$$P_{eq} \approx 57 \text{ s} \Big(\frac{M_\odot}{M}\Big)^{5/7} \Big(\frac{10^{-8} M_\odot/\text{yr}}{\dot{M}}\Big)^{3/7} \times \Big(\frac{B}{10^5 \text{G}}\Big)^{6/7} \Big(\frac{R}{7.0\times 10^8 \text{cm}}\Big)^{18/7}. \quad (13)$$

The observed periods of Dwarf Novae Oscillations (DNOs) are in the range of $7-70$ s (Warner, 2004).

5.3. *Millisecond Pulsars*

Our simulations are also applicable to millisecond X-ray pulsars, which are the accreting low-magnetic-field neutron stars (van der Klis, 2000). The period of such a star in the rotational equilibrium is

$$P_{eq} \approx 1.8 \text{ ms} \Big(\frac{1.4 M_\odot}{M}\Big)^{5/7} \Big(\frac{10^{-9} M_\odot/\text{yr}}{\dot{M}}\Big)^{3/7} \times \Big(\frac{B}{10^8 \text{G}}\Big)^{6/7} \Big(\frac{R}{10^6 \text{cm}}\Big)^{18/7}. \quad (14)$$

For all accretion-powered millisecond X-ray pulsars we have known, the spin frequencies range from 185Hz to 435Hz (Wijnands, R. 2004), or, the spin rate is in range of 2.3-5.2 ms. These values may be obtained from Eqn.14 at smallere $\dot{M}$ or larger B.

6. DISCUSSION

We investigated the conditions for the rotational equilibrium or"torqueless" accretion state using axisymmetric MHD simulations. In such a state the total angular momentum flux to the star is approximately zero. We found the equilibrium states by gradually changing the angular velocity of the star with the other parameters fixed. We considered two main cases: One with relatively low magnetic field and dense corona and second with much stronger field and lower density corona. We observed that in both cases the rotation of the star is approximately locked to the rotation of the inner radius of the disk such that a star rotates somewhat slower than the inner radius of the disk. In the first case the ratio between corotation radius of the star and the Alfvén radius r_A (where the disk is disrupted) is $r_{co}/r_A \sim 1.3-1.4$. In the second case, where stronger inflation of the magnetic field was observed, this ratio is only slightly larger, $r_{co}/r_A \sim 1.4-1.5$. We observed that in the first case, the angular momentum transport is associated with the closed field lines at the inner radii of the disk. Open field lines spin down the star, but the role of this spin-down is small. In the second case outflow of angular momentum along the inflated field lines is more significant than in the first case, however this did not change the result, which probably means that the angular momentum transport associated with the inner regions of the disk and the region of the funnel flow is more significant. Thus, in both cases the magnetic interaction effectively locks the rotation rate of the star to a value which depends mainly on the mass accretion rate and the star's magnetic moment. We should note that most of coronal region is still matter dominated. This is connected with the fact that the magnetic energy-density of the dipole decreases with distance as $\sim R^{-6}$ so that it is difficult to set up a magnetically dominated corona. Goodson et al. (1997, 1999) were able to model such a corona by arranging fast fall-off of coronal density with the distance. However, their initial conditions are sufficiently far from equilibrium that the torqueless accretion was not established. Future simulations with even lower coronal densities will help to understand whether a star is always locked to the rotation rate of the inner radius of the disk. Our simulations for two very different initial conditions have shown very similar results for the rotational equilibrium which may be a sign that the disk-locking may be a similar for all slowly rotating stars.

We applied our simulation results to Classical T Tauri stars, where disk locking may explain their slow rotation. Also, we estimated the probable periods of rotation of other accretion powered systems, such as dwarf novae and X-ray millisecond pulsars.

The authors thank Drs. Koldoba and Ustyugova for developing of codes and helpful discussions. This work was supported in part by NASA grants NAG 5-13220, NAG 5-13060 and by NSF grant AST-0307817.

REFERENCES

Agapitou, V., & Papaloizou, J. C. B. 2000, MNRAS, 317, 273
Attridge, J. M., & Herbst, W. 1992, ApJ, 398, L61
Bardou, A. 1999, MNRAS, 306, 669
Bouvier, J.Cabrit, S.,Fernández, M., Martín, E.L., & Matthews, J. M. 1993, A&A, 272,176
Bildsten, L., et al. 1997, ApJS, 113, 367
Camenzind, M. 1990, Rev. Mod. Astron., 3, 234
Davidson, K., & Ostriker, J. P. 1973, ApJ, 179, 585
Edwards, S., et al. 1993, AJ, 106, 372
Elsner, R. F., and Lamb, F. K. 1977, ApJ, 215, 897
Fendt, C., & Elstner, D. 1999, A&A, 349, L61
Ghosh, P., & Lamb, F. K. 1978, ApJ, 223, L83
Ghosh, P., Lamb, F. K. 1979, ApJ, 234, 296
Ghosh, P., Lamb, F. K., & Pethick, C. J. 1977, ApJ, 217, 578
Goodson, A. P., Böhm, K. H., & Winglee, R. 1999, ApJ, 524, 142
Goodson, A. P., Winglee, R., & Böhm, K. H. 1997, ApJ, 489, 199
Hayashi, M. R., Shibata, K., & Matsumoto, R. 1996, ApJ, 468, L37
Hirose, S., Uchida, Y., Shibata, K., & Matsumoto, R. 1997, PASJ, 49, 193
Kato, Y., Hayashi, M. R., & Matsumoto, R. 2004, ApJ, 600, 338
Kenyon, S. J., Yi, I. & Hartmann, L. 1996, ApJ, 462,439
Koldoba, A. V., Kuznetzov, O. A., & Ustyugova, G. V. 1992, Rep. Keldysh Inst. Applied Mathematics, Russian Acad. Sci., No. 69
Koldoba, A. V., Lovelace, R. V. E., Ustyugova, G. V., & Romanova, M. M. 2002, AJ, 123, 2019
Koldoba, A. V., & Ustyugova, G. V. 1994, Rep. Keldysh Inst. Applied Mathematics, Russian Acad. Sci., No. 87
Königl, A. 1991, ApJ, 370, L39
Lamb, F. K., Pethick, C. J., & Pines, D. 1973, ApJ, 184, 271
Li, J., & Wickramasinghe, D. T. 1997, MNRAS, 286, L25
Lovelace, R. V. E., Romanova, M. M., & Bisnovatyi-Kogan, G. S. 1995, MNRAS, 275, 244
Matt, S., & Pudritz, R .E. 2004, ApJ, 607, L43
Matt, S., & Pudritz, R .E. 2005, MNRAS, 356, 167
Miller, K. A., & Stone, J. M. 1997, ApJ, 489, 890
Nagase, F. 1989, PASJ, 41, 1
Pringle, J. E., & Rees, M. J. 1972, A&A, 21, 1
Romanova, M. M., Ustyugova, G. V., Koldoba, A. V., Chechetkin, V. M., & Lovelace, R. V. E. 1998, ApJ, 500, 703

Romanova, M. M., Ustyugova, G. V., Koldoba, A. V., & Lovelace, R. V. E. 2002, ApJ, 578, 420
Romanova, M. M., Ustyugova, G. V., Koldoba, A. V., & Lovelace, R. V. E. 2004, ApJ, 616, L151
Shakura, N. I., & Sunyaev, R. A. 1973, A&A, 24, 337
Shu, F. H., Najita, J., Ruden, S. P., & Lizano, S. 1994, ApJ, 429, 797
Ustyugova, G. V., Koldoba, A. V., Romanova, M. M., Chechetkin, V. M., & Lovelace, R. V. E. 1995, ApJ, 439, L39
———. 1999, ApJ, 516, 221
Uzdensky, D.A., Königl, A., & Litwin, C. 2002, ApJ, 565, 1191
van der Klis, M. 2000, Annu. Rev. Astron. Astrophys, 38, 717
Von Rekowski, B. & Brandenburg, A. 2004, A&A, 420, 17
Wang, Y.-M. 1995, ApJ, 449, L153
Warner, B. 1995, Cataclysmic Variable Stars (Cambridge: Cambridge Univ. Press)
Warner, B. 2004, PASP, 116, 115
Wijnands R., 2004, in Kaaret P., Lamb F. K., Swank J. H., eds, AIP Conf. Proc. Vol. 714, X-ray Timing 2003: Rossi and Beyond. Am. Inst. Phys., Melville, NY, p. 209